

Study of the process $e^+e^- \rightarrow \pi^+\pi^-$ in the energy region $400 < \sqrt{s} < 1000$ MeV.

M.N.Achasov,* K.I.Beloborodov, A.V.Berdyugin, A.G.Bogdanchikov, A.V.Bozhenok,
A.D.Bukin, D.A.Bukin, T.V.Dimova, V.P.Druzhinin, V.B.Golubev, I.A.Koop,
A.A.Korol, S.V.Koshuba, A.P.Lysenko, A.V.Otboev, E.V.Pakhtusova, S.I.Serednyakov,
Yu.M.Shatunov, V.A.Sidorov, Z.K.Silagadze, A.N.Skrinsky, Yu.A.Tikhonov, and A.V.Vasiljev
*Budker Institute of Nuclear Physics,
Siberian Branch of the Russian Academy of Sciences
11 Lavrentyev, Novosibirsk, 630090, Russia
Novosibirsk State University,
630090, Novosibirsk, Russia*

The cross section of the process $e^+e^- \rightarrow \pi^+\pi^-$ was measured in the SND experiment at the VEPP-2M collider in the energy region $400 < \sqrt{s} < 1000$ MeV. This measurement was based on about 12.4×10^6 selected collinear events, which include 7.4×10^6 $e^+e^- \rightarrow e^+e^-$, 4.5×10^6 $e^+e^- \rightarrow \pi^+\pi^-$ and 0.5×10^6 $e^+e^- \rightarrow \mu^+\mu^-$ selected events. The systematic uncertainty of the cross section determination is 1.3 %. The ρ -meson parameters were determined: $m_\rho = 774.9 \pm 0.4 \pm 0.5$ MeV, $\Gamma_\rho = 146.5 \pm 0.8 \pm 1.5$ MeV, $\sigma(\rho \rightarrow \pi^+\pi^-) = 1220 \pm 7 \pm 16$ nb as well as the parameters of the G -parity suppressed decay $\omega \rightarrow \pi^+\pi^-$: $\sigma(\omega \rightarrow \pi^+\pi^-) = 29.9 \pm 1.4 \pm 1.0$ nb and $\phi_{\rho\omega} = 113.5 \pm 1.3 \pm 1.7$ degree.

PACS numbers: 13.66Bc, 13.66Jn, 13.25Jx, 12.40Vv

I. INTRODUCTION

The cross section of the $e^+e^- \rightarrow \pi^+\pi^-$ process in the energy region $\sqrt{s} < 1000$ MeV can be described within the vector meson dominance model (VDM) framework and is determined by the transitions $V \rightarrow \pi^+\pi^-$ of the light vector mesons ($V = \rho, \omega, \rho', \rho''$) into the final state. The main contribution in this energy region comes from the $\rho \rightarrow \pi^+\pi^-$ and from the G -parity violating $\omega \rightarrow \pi^+\pi^-$ transitions. Studies of the $e^+e^- \rightarrow \pi^+\pi^-$ reaction allow us to determine the ρ and ω meson parameters and provide information on the G -parity violation mechanism.

At low energies the $e^+e^- \rightarrow \pi^+\pi^-$ cross section gives the dominant contribution to the celebrated ratio $R(s) = \sigma(e^+e^- \rightarrow \text{hadrons})/\sigma(e^+e^- \rightarrow \mu^+\mu^-)$, which is used for calculation of the dispersion integrals. For example, for evaluation of the electromagnetic running coupling constant at the Z -boson mass $\alpha_{em}(s = m_Z^2)$, or for determination of the hadronic contribution a_μ^{hadr} to the anomalous magnetic moment of the muon, which nowadays is measured with very high accuracy 5×10^{-6} [1, 2].

Assuming conservation of the vector current (CVC) in the isospin symmetry limit, the spectral function of the $\tau^\pm \rightarrow \pi^\pm \pi^0 \nu_\tau$ decay can be related to the isovector part of the $e^+e^- \rightarrow \pi^+\pi^-$ cross section. The spectral function was determined with high precision in Ref.[3, 4, 5]. The comparison of the $e^+e^- \rightarrow \pi^+\pi^-$ cross section with what follows from the spectral function provides an accurate test of the CVC hypothesis.

The process $e^+e^- \rightarrow \pi^+\pi^-$ in the energy region $\sqrt{s} < 1000$ MeV was studied in several experiments [6, 7, 8, 9, 10, 11, 12, 13, 14, 15, 16, 17, 18, 19] during more than 30 years. In present work the results of the $e^+e^- \rightarrow \pi^+\pi^-$ cross section measurement with SND detector at $390 \leq \sqrt{s} \leq 980$ MeV are reported.

II. EXPERIMENT

The SND detector [20] operated from 1995 to 2000 at the VEPP-2M [21] collider in the energy range \sqrt{s} from 360 to 1400 MeV. The detector contains several subsystems. The tracking system includes two cylindrical drift chambers. The three-layer spherical electromagnetic calorimeter is based on NaI(Tl) crystals. The muon/veto system consists of plastic scintillation counters and two layers of streamer tubes. The calorimeter energy and angular resolutions depend on the photon energy as $\sigma_E/E(\%) = 4.2\%/\sqrt[4]{E(\text{GeV})}$ and $\sigma_{\phi,\theta} = 0.82^\circ/\sqrt{E(\text{GeV})} \oplus 0.63^\circ$. The tracking system angular resolution is about 0.5° and 2° for azimuthal and polar angles respectively.

*Electronic address: achasov@inp.nsk.su

In 1996 – 2000 the SND detector collected data in the energy region $\sqrt{s} < 980$ MeV with integrated luminosity about 10.0 pb^{-1} . The beam energy was calculated from the magnetic field value in the bending magnets of the collider. The accuracy of the energy setting is about 0.1 MeV. The beam energy spread varies in the range from 0.06 MeV at $\sqrt{s} = 360$ MeV to 0.35 MeV at $\sqrt{s} = 970$ MeV.

III. DATA ANALYSIS

The cross section of the $e^+e^- \rightarrow \pi^+\pi^-$ process was measured in the following way.

1. The collinear events $e^+e^- \rightarrow e^+e^-, \pi^+\pi^-, \mu^+\mu^-$ were selected;
2. The selected events were sorted into the two classes: e^+e^- and $\pi^+\pi^-, \mu^+\mu^-$ using the energy deposition in the calorimeter layers;
3. The $e^+e^- \rightarrow e^+e^-$ events were used for integrated luminosity determination. The events of the $e^+e^- \rightarrow \mu^+\mu^-$ process were subtracted according to the theoretical cross section, integrated luminosity and detection efficiency;
4. In order to determine the cross section of the $e^+e^- \rightarrow \pi^+\pi^-$ process, the number of $e^+e^- \rightarrow \pi^+\pi^-$ events in each energy point were normalized on the integrated luminosity and divided by the detection efficiency and radiative correction.

The detection efficiency was obtained from Monte Carlo (MC) simulation [20]. The MC simulation of SND is based on UNIMOD [22] package. The SND geometrical model description comprises about 10000 distinct volumes and includes details of the SND design. The primary generated particles are tracked through the detector media taking into account the following effects: ionization losses, multiple scattering, bremsstrahlung of electrons and positrons, Compton effect and Rayleigh scattering, e^+e^- pair production by photons, photo-effect, unstable particles decays, interaction of stopped particles, nuclear interaction of hadrons [23, 24, 25]. After that the signals produced in each detector element are simulated. The electronics noise, signals pile up, the actual time and amplitude resolutions of the electronics channels and broken channels were taken into account during processing the Monte Carlo events to provide the adaptable account of variable experimental conditions.

The MC simulation of the processes $e^+e^- \rightarrow e^+e^-, \mu^+\mu^-, \pi^+\pi^-$ was based on the formula obtained in the Ref.[26, 27, 28]. The simulation of the process $e^+e^- \rightarrow e^+e^-$ was performed with the cut $30^\circ < \theta_{e^\pm} < 150^\circ$ on the polar angles of the final electron and positron.

The $e^+e^- \rightarrow e^+e^-, \mu^+\mu^-$ and $\pi^+\pi^-$ events are differed by energy deposition in the calorimeter. In $e^+e^- \rightarrow e^+e^-$ events the electrons produce the electromagnetic shower with the most probable energy losses about 0.92 of the initial particle energy. The distributions of the energy deposition of the electrons with the different energies are shown in Fig.1. The experimental and simulated spectra are in good agreement. Muons lose their energy by ionization of the calorimeter material through which they pass and their energy deposition spectra are well modeled in simulation (Fig.2). The similar ionization losses are experienced by charged pions and this part of the charged pion energy deposition is well described by simulation (Fig.3). But pions lose their energy also due to nuclear interactions which is not so accurately reproduced in simulation. This leads to some difference in energy deposition spectra in experiment and simulation for charged pions (Fig.4).

The discrimination between electrons and pions in the SND detector is based on difference in longitudinal energy deposition profiles (deposition in calorimeter layers) for these particles. To use in the most complete way the correlations between energy depositions in the calorimeter layers, the corresponding separation parameter was based on the neural network approach [29]. For each energy point the neural network – multilayer perceptron was constructed. The network had input layer consisting of 7 neurons, two hidden layers with 20 neurons each and the output layer with one neuron. As the input data the network used the energy depositions of the particles in calorimeter layers and the polar angle of one of the particles. The output signal $R_{e/\pi}$ is a number in the interval from -0.5 to 1.5. The network was trained by using simulated $e^+e^- \rightarrow \pi^+\pi^-$ and $e^+e^- \rightarrow e^+e^-$ events. The distribution of the discrimination parameter $R_{e/\pi}$ is shown in Fig.5. The $e^+e^- \rightarrow e^+e^-$ events are located in the region $R_{e/\pi} > 0.5$, while $e^+e^- \rightarrow \pi^+\pi^-, \mu^+\mu^-$ events at $R_{e/\pi} < 0.5$.

A. Selection criteria

During the experimental runs, the first-level trigger [20] selects events with one or more tracks in tracking system and with two clusters in calorimeter with the spatial angle between the clusters more than 100° . The threshold on energy deposition in cluster was equal to 25 MeV. The threshold on the total energy deposition in the calorimeter

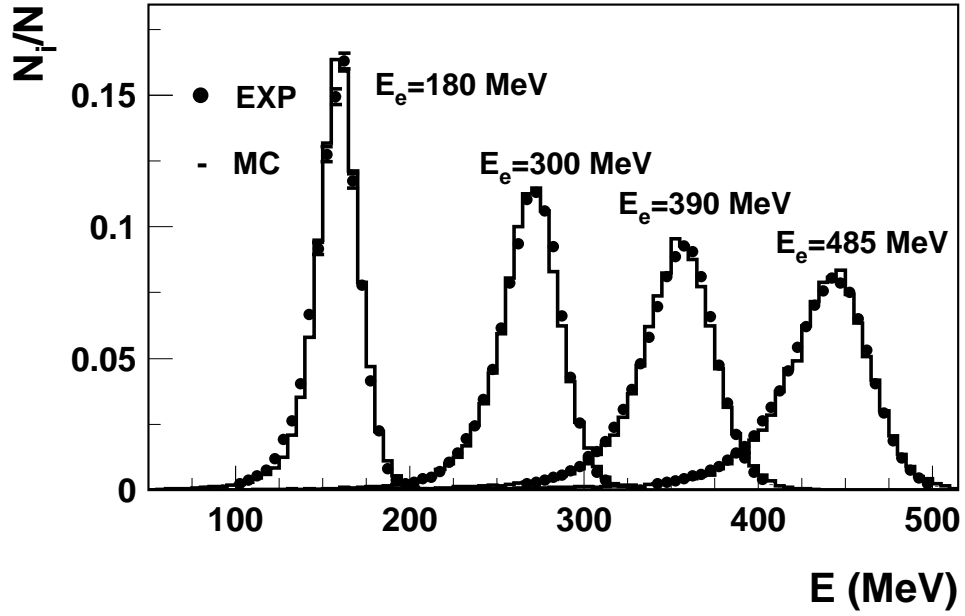


FIG. 1: Energy deposition spectra for electrons with the energies 180, 300, 390 and 485 MeV in experiment (dots) and simulation (histogram).

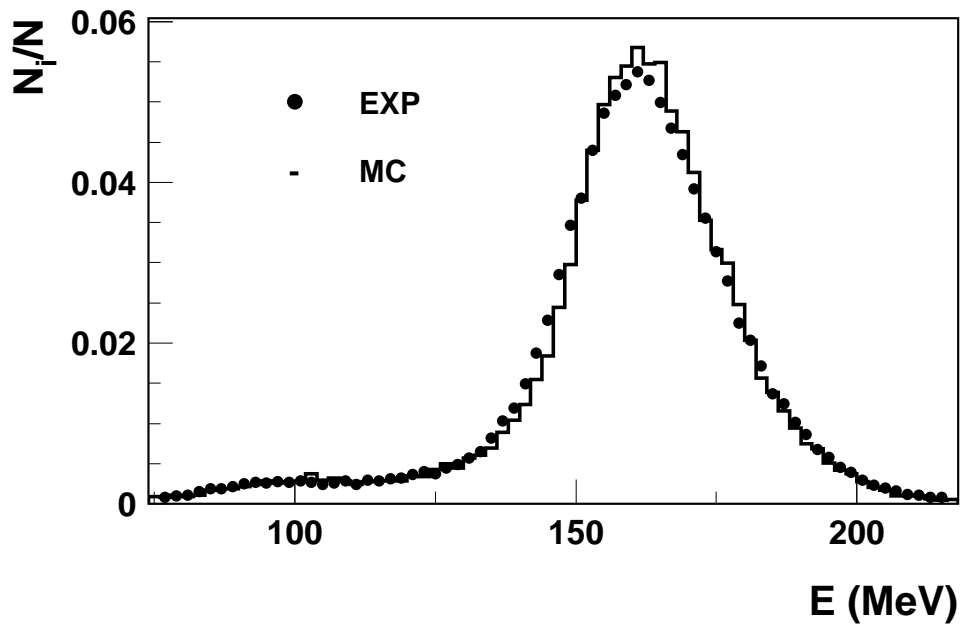


FIG. 2: Energy deposition spectra for the 500 MeV muons in experiment (dots) and simulation (histogram).

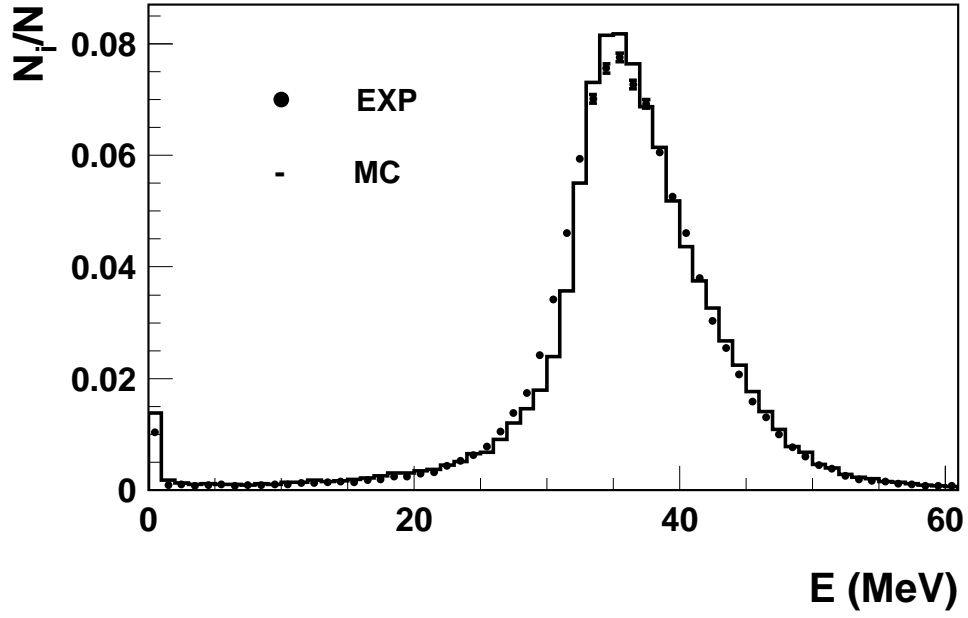


FIG. 3: The spectra of the ionization losses of the pions with energy $E_\pi > 360$ MeV in the first calorimeter layer. Dots – experiment, histogram – simulation.

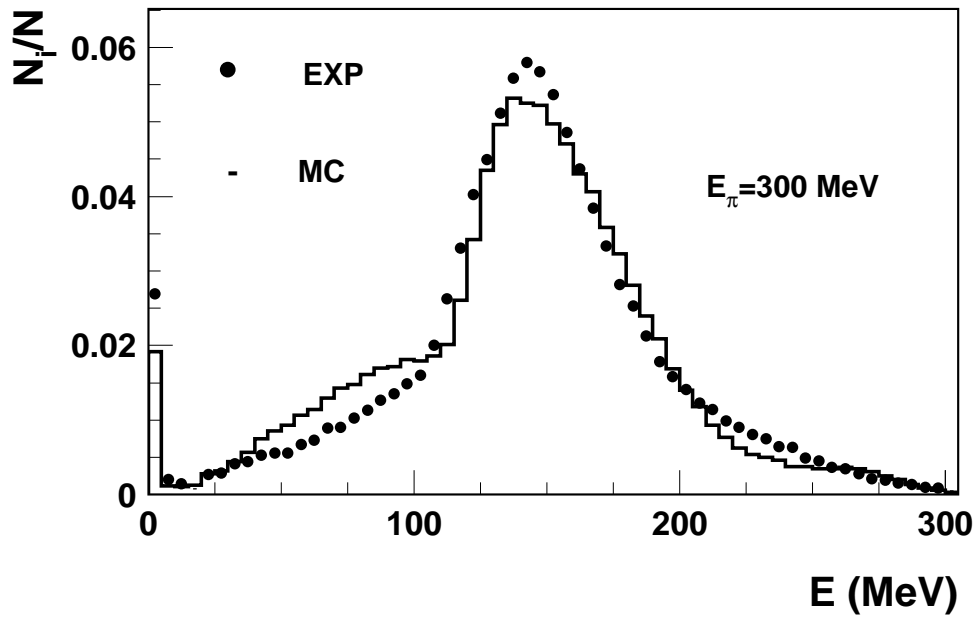


FIG. 4: Energy deposition spectra of the pions with the energy $E_\pi = 300$ MeV. Dots – experiment, histogram – simulation.

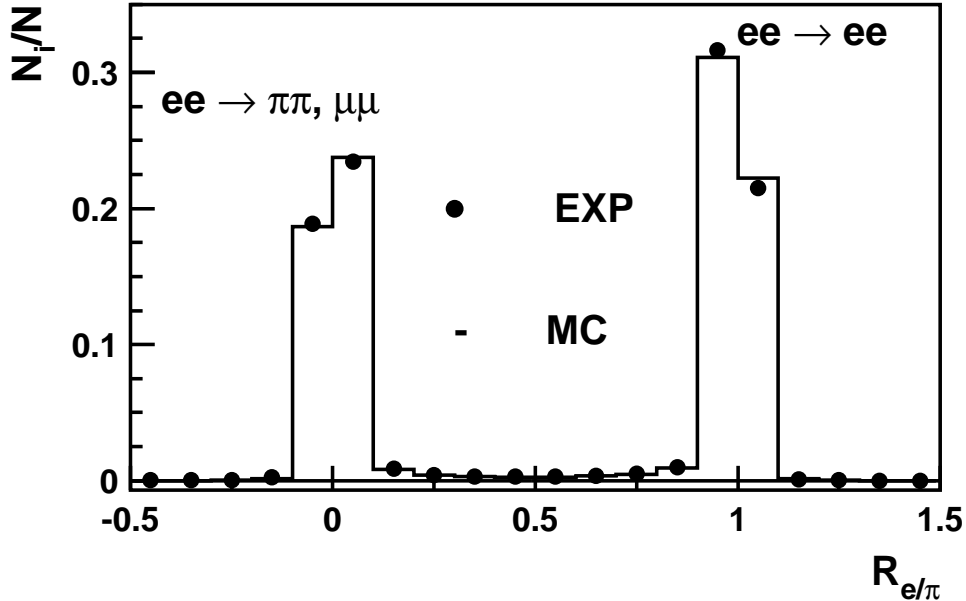


FIG. 5: The e/π discrimination parameter distribution for all collinear events in the energy region \sqrt{s} from 880 to 630 MeV. Dots – experiment, histogram – simulation.

was set equal to 140 MeV in the energy region $\sqrt{s} \geq 850$ MeV, and to 100 MeV, or was absent at all, below 850 MeV. During processing of the experimental data the event reconstruction is performed [20, 30]. For further analysis, events containing two charged particles with $|z| < 10$ cm and $r < 1$ cm were selected. Here z is the coordinate of the charged particle production point along the beam axis (the longitudinal size of the interaction region depends on beam energy and varies from 1.5 to 2.5 cm); r is the distance between the charged particle track and the beam axis in the $r - \phi$ plane. The polar angles of the charged particles were bounded by the criterion: $55^\circ < \theta < 125^\circ$ and the energy deposition of each of them was required to be greater than 50 MeV. The following cuts on the acollinearity angles in the azimuthal and polar planes were applied: $|\Delta\phi| < 10^\circ$ and $|\Delta\theta| < 10^\circ$. In the event sample selected under these conditions one has the $e^+e^- \rightarrow e^+e^-, \pi^+\pi^-, \mu^+\mu^-$ events, cosmic muons background and a small contribution from the $e^+e^- \rightarrow \pi^+\pi^-\pi^0$ reaction at $\sqrt{s} \simeq m_\omega$. The muon system *veto* was used for suppression of the cosmic muon background (*veto* = 0).

B. The background from the cosmic muons and from the $e^+e^- \rightarrow \pi^+\pi^-\pi^0$ process.

The number of background events from the $e^+e^- \rightarrow \pi^+\pi^-\pi^0$ process was estimated in the following way:

$$N_{3\pi}(s) = \sigma_{3\pi}(s)\epsilon_{3\pi}(s)IL(s), \quad (1)$$

where $\sigma_{3\pi}(s)$ is the cross section of the $e^+e^- \rightarrow \pi^+\pi^-\pi^0$ process with the radiative corrections taken into account, $IL(s)$ is the integrated luminosity, $\epsilon_{3\pi}(s)$ is the detection probability for the background process obtained from the simulation under the selection criteria described above. The values of $\sigma_{3\pi}(s)$ were taken from the SND measurements [31]. Although $\sigma_{3\pi}(m_\omega) \approx 1300$ nb, the $e^+e^- \rightarrow 3\pi$ process contribution to the total number of the collinear events at the ω resonance peak is less than 0.3 %. The leading role in the suppression of this background was played by the cuts on the acollinearity angles $\Delta\theta$ and $\Delta\phi$. In order to check the estimation (1), the events containing two and more photons with energy depositions more than 200 MeV were considered. The constraint on the photons energy deposition greatly suppresses not the $e^+e^- \rightarrow 3\pi$ events, as a result of the fact that our selection criteria select the

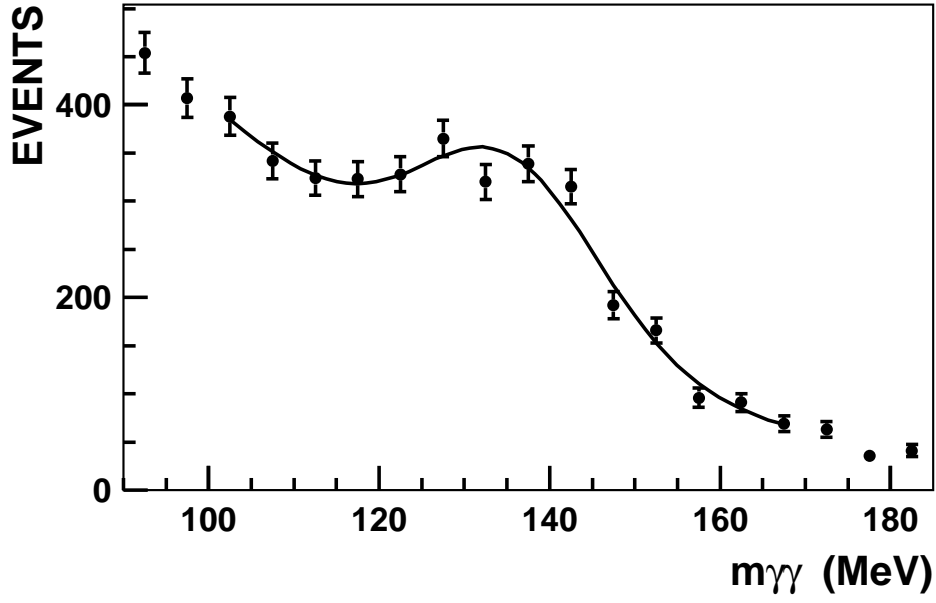


FIG. 6: Two-photon invariant mass $m_{\gamma\gamma}$ distribution at $\sqrt{s} \simeq m_\omega$.

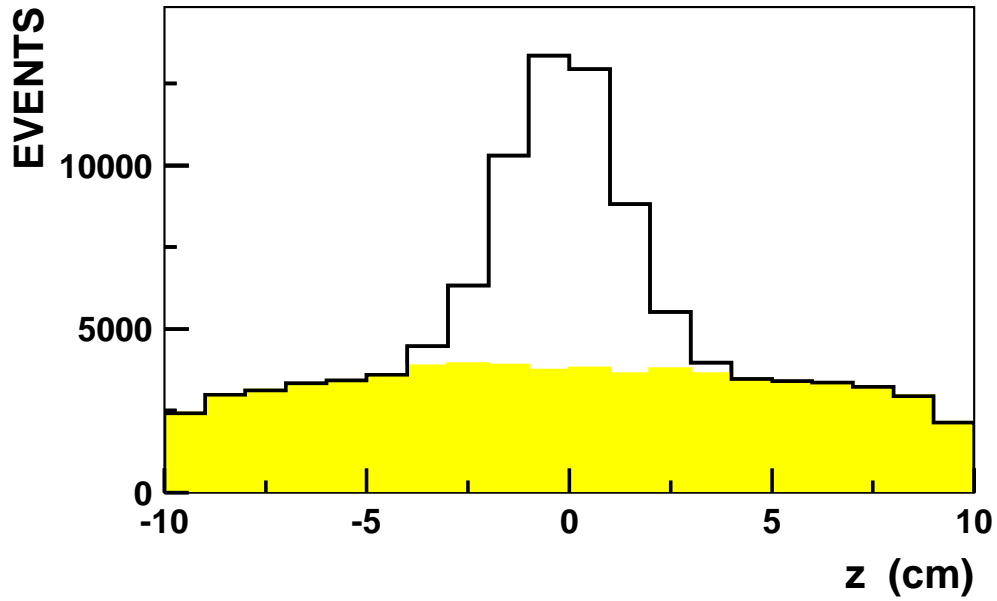


FIG. 7: The distribution of the z coordinate of the charged particle production point along the beam axis for collinear events at $\sqrt{s} = 180$ MeV. Histogram – all events, dashed distribution – events with muon system veto ($veto = 1$).

$e^+e^- \rightarrow 3\pi$ events with collinear charged pions and therefore the neutral pion in this events has relatively low energy. In order to obtain $e^+e^- \rightarrow 3\pi$ events number $n_{3\pi}$, the invariant mass spectrum $m_{\gamma\gamma}$ (Fig.6) was fitted by the sum of Gaussian and the second order polynomial: $G(m_{\gamma\gamma}) \times n_{3\pi} + P_2(m_{\gamma\gamma}) \times (n - n_{3\pi})$. The value of $n_{3\pi}$ agrees with events number calculated according to (1).

The cosmic muon background was suppressed by the muon/veto system. The z coordinate distribution for the charged particle production point along the beam axis is shown in Fig.7 for collinear events. The e^+e^- annihilation events have the Gaussian distribution peaked at $z = 0$, while the cosmic background distribution is nearly uniform and clearly extends outside the peak. As the Fig.7 shows, the muon system *veto* ($veto = 1$) separates cosmic muons from the e^+e^- annihilation events. The residual events number of the cosmic muon background was estimated from the following formula:

$$N_\mu = \nu_\mu \times T. \quad (2)$$

Here $\nu_\mu \simeq 1.3 \times 10^{-3}$ Hz is the frequency of cosmic background registration under the applied selection criteria, T is the time of data taking. The value of ν_μ was obtained by using data collected in special runs without beams in collider. The first-level trigger counting rate in these runs was 2 Hz. The contribution of the cosmic background to the total number of selected collinear events depends on energy \sqrt{s} and varies from 0.1 % to 1 %.

The $e^+e^- \rightarrow \pi^+\pi^-\pi^0$ events are concentrated in the $R_{e/\pi}$ discrimination parameter region $R_{e/\pi} < 0.5$. The cosmic background events at the energies $\sqrt{s} > 600$ also fall in the area $R_{e/\pi} < 0.5$, because the energy deposition of the cosmic muons is much lower than the energy deposition in the $e^+e^- \rightarrow e^+e^-$ events. For the lower center of mass energies the cosmic background moves to the area $R_{e/\pi} > 0.5$, because in this case the energy depositions are close.

C. Detection efficiency

The $\Delta\phi$ and $\Delta\theta$ distributions of the $e^+e^- \rightarrow e^+e^-$ and $e^+e^- \rightarrow \pi^+\pi^-$ events are shown in Fig.8,9, 10 and 11. Experiment and simulation agree rather well. As a measure of systematic uncertainty due to $\Delta\theta$ cut the following value was used:

$$\delta_{\Delta\theta} = \frac{\delta_{\pi\pi}^{\Delta\theta}}{\delta_{ee}^{\Delta\theta}}, \quad (3)$$

where

$$\delta_{\Delta\theta}^x = \frac{n_x(|\Delta\theta| < 10^\circ)}{N_x(|\Delta\theta| < 20^\circ)} / \frac{m_x(|\Delta\theta| < 10^\circ)}{M_x(|\Delta\theta| < 20^\circ)}, \quad x = \pi\pi(ee).$$

Here $n_x(|\Delta\theta| < 10^\circ)$ and $m_x(|\Delta\theta| < 10^\circ)$ are the numbers of experimental and simulated events, selected under the condition $|\Delta\theta| < 10^\circ$, while $N_x(|\Delta\theta| < 20^\circ)$ and $M_x(|\Delta\theta| < 20^\circ)$ are the numbers of experimental and simulated events with $|\Delta\theta| < 20^\circ$. The $\delta_{\Delta\theta}$ does not depend on energy, its average value is equal to 0.999 and it has systematic spread of 0.4 %. This systematic spread was added to the error of the cross section measurement in each energy point. Systematic error due to the $\Delta\phi$ cut is significantly lower and was neglected.

The polar angle distributions for the $e^+e^- \rightarrow e^+e^-$ and $e^+e^- \rightarrow \pi^+\pi^-$ processes are shown in Fig.12 and 13. The ratio of these θ distributions is shown in Fig.14. The experimental and simulated distributions are in agreement. In order to estimate the systematic inaccuracy due to the θ angle selection cut the following ratio was used:

$$\delta_\theta = \frac{\delta(\theta_x)}{\delta(55^\circ)}, \quad (4)$$

where

$$\delta(\theta_x) = \frac{N_{\pi\pi}(\theta_x < \theta < 180^\circ - \theta_x)}{N_{ee}(\theta_x < \theta < 180^\circ - \theta_x)} / \frac{M_{\pi\pi}(\theta_x < \theta < 180^\circ - \theta_x)}{M_{ee}(\theta_x < \theta < 180^\circ - \theta_x)}, \quad 50^\circ < \theta_x < 90^\circ.$$

Here $N_{\pi\pi}(\theta_x < \theta < 180^\circ - \theta_x)$, $N_{ee}(\theta_x < \theta < 180^\circ - \theta_x)$, $M_{\pi\pi}(\theta_x < \theta < 180^\circ - \theta_x)$, $M_{ee}(\theta_x < \theta < 180^\circ - \theta_x)$ are the experimental and simulated $e^+e^- \rightarrow \pi^+\pi^-$ and $e^+e^- \rightarrow e^+e^-$ event numbers in the angular range $\theta_x < \theta < 180^\circ - \theta_x$. The maximal difference of δ_θ from unity was found to be 0.8%. This value was taken as a systematic error $\sigma_\theta = 0.8\%$ associated with the angular selection cut.

In the tracking system the particle track can be lost due to reconstruction inefficiency. The probabilities to find the track was determined by using experimental data themselves. It was found to be $\varepsilon_e \simeq 0.996$ for electrons and

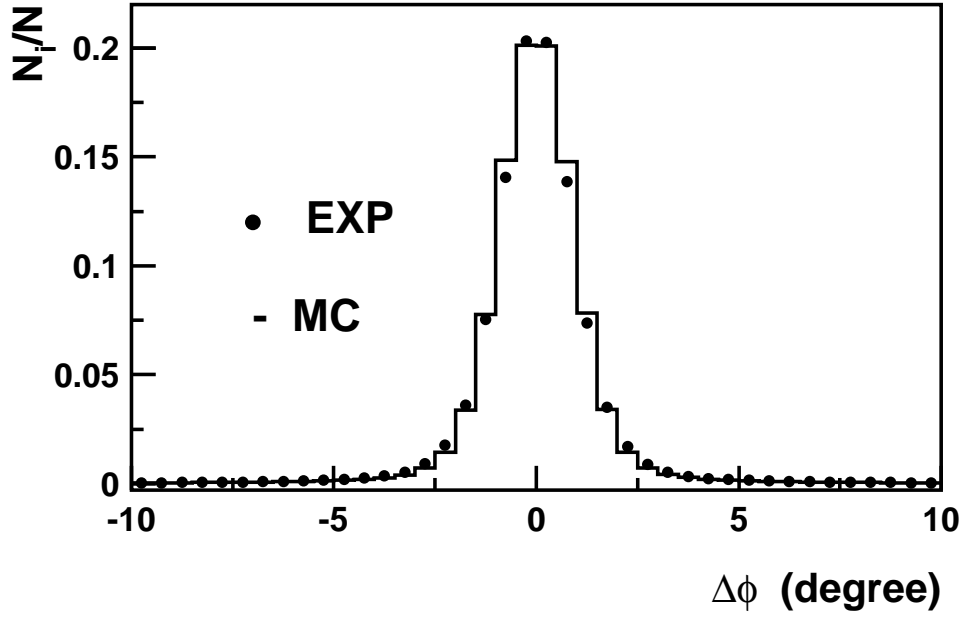


FIG. 8: The $\Delta\phi$ distribution of the $e^+e^- \rightarrow e^+e^-$ events. Dots – experiment, histogram – simulation.

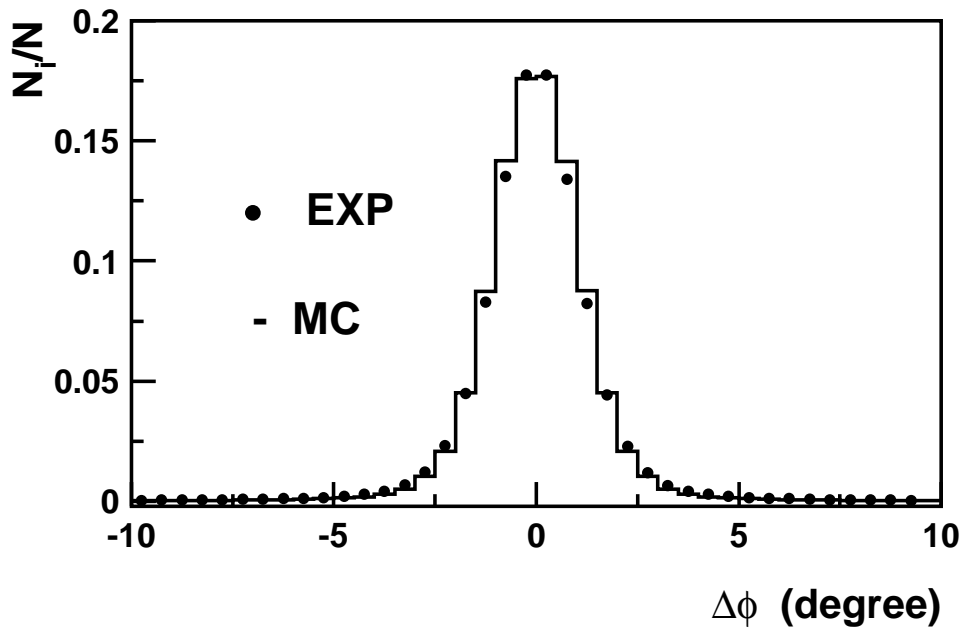


FIG. 9: The $\Delta\phi$ distribution of the $e^+e^- \rightarrow \pi^+\pi^-$ events. Dots – experiment, histogram – simulation.

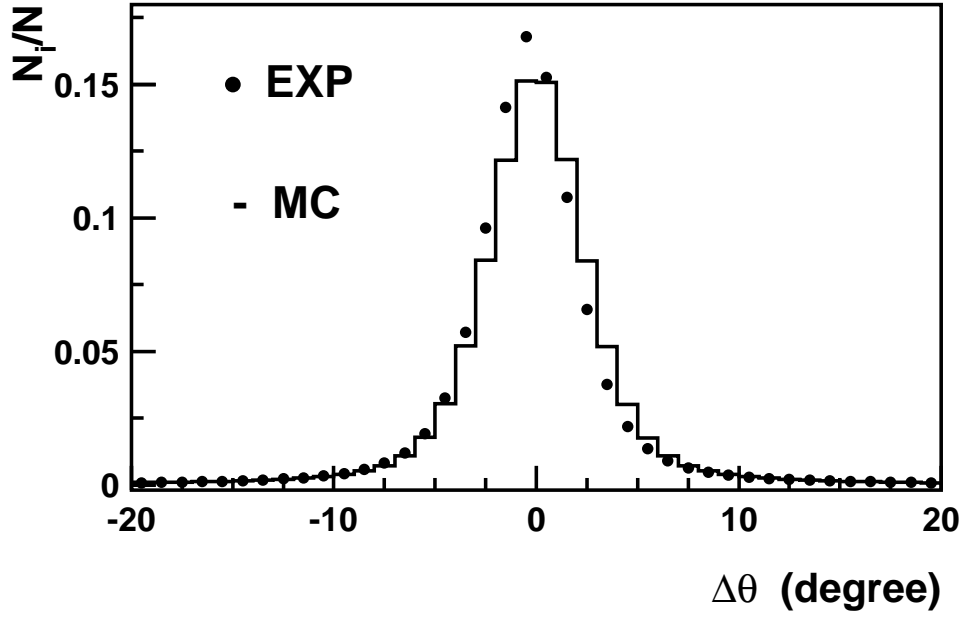


FIG. 10: The $\Delta\theta$ distribution of the $e^+e^- \rightarrow e^+e^-$ events. Dots – experiment, histogram – simulation.

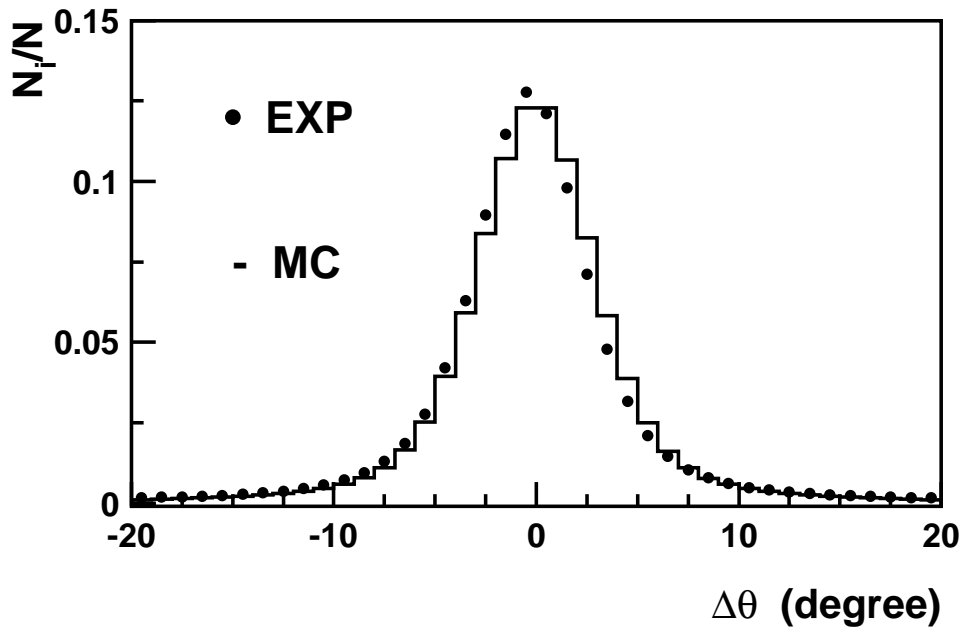


FIG. 11: The $\Delta\theta$ distribution of the $e^+e^- \rightarrow \pi^+\pi^-$ events. Dots – experiment, histogram – simulation.

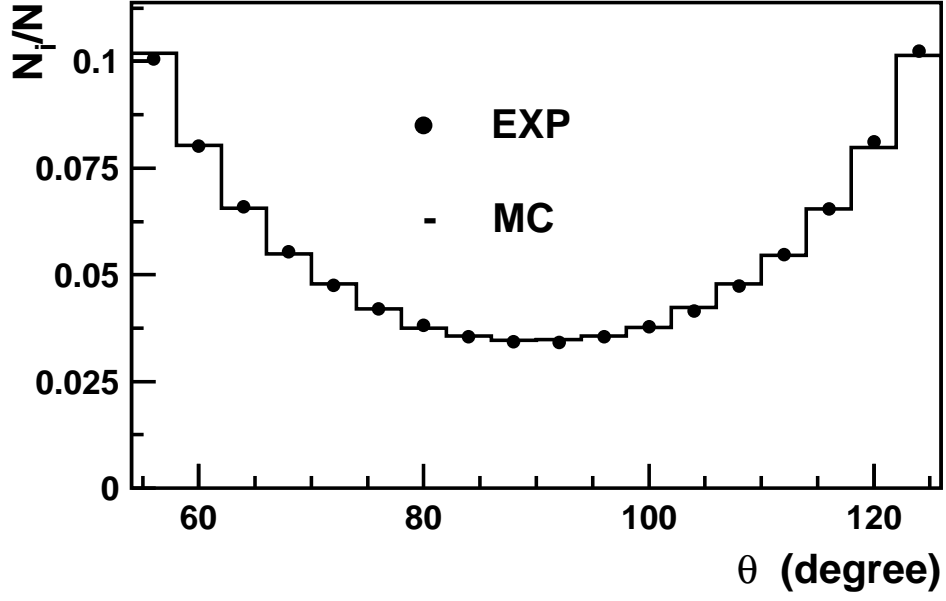


FIG. 12: The θ angle distribution of the $e^+e^- \rightarrow e^+e^-$ events. Dots – experiment, histogram – simulation.

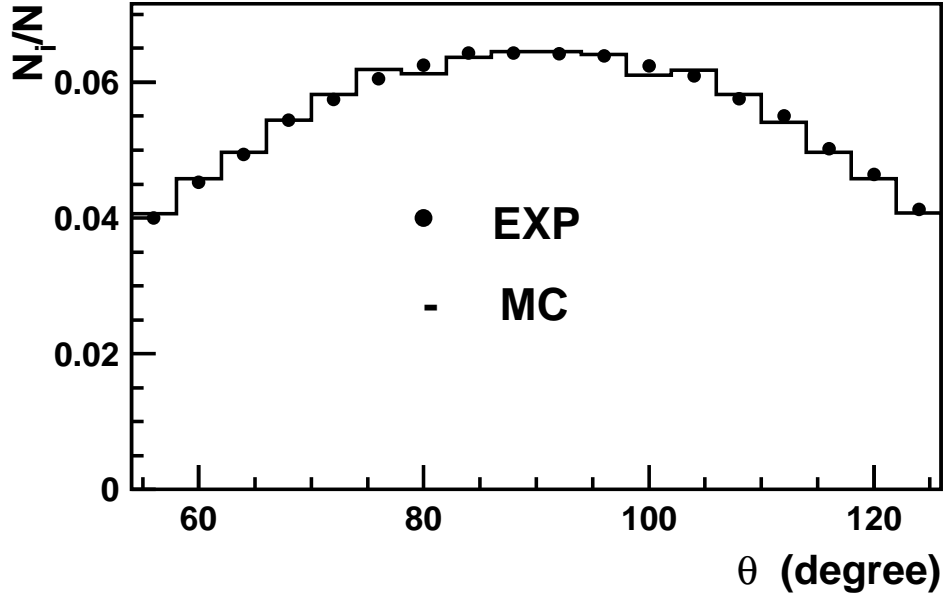


FIG. 13: The θ angle distribution of the $e^+e^- \rightarrow \pi^+\pi^-$ events. Dots – experiment, histogram – simulation.

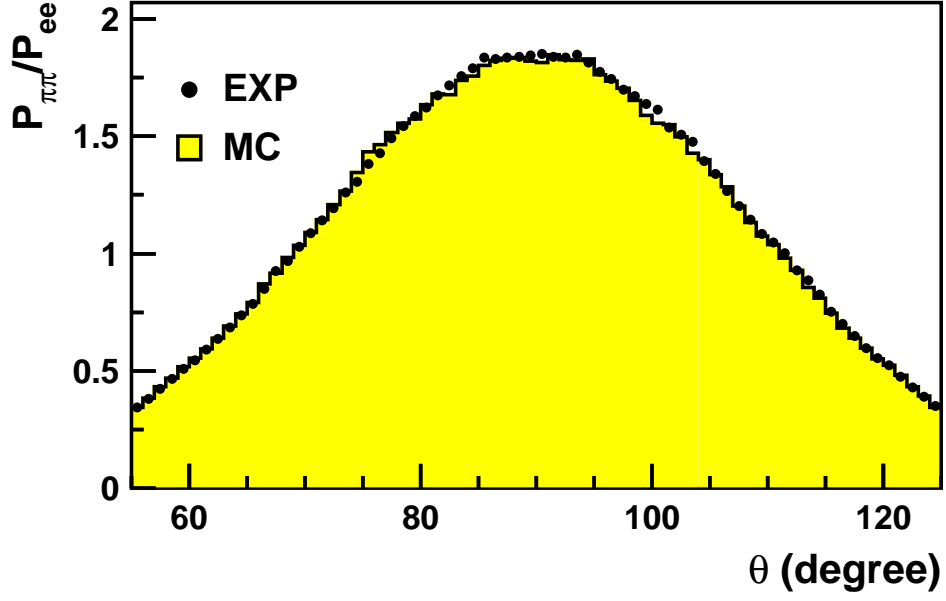


FIG. 14: The ratio of θ distributions of the $e^+e^- \rightarrow \pi^+\pi^-$ and $e^+e^- \rightarrow e^+e^-$ processes. Dots – experiment, histogram – simulation.

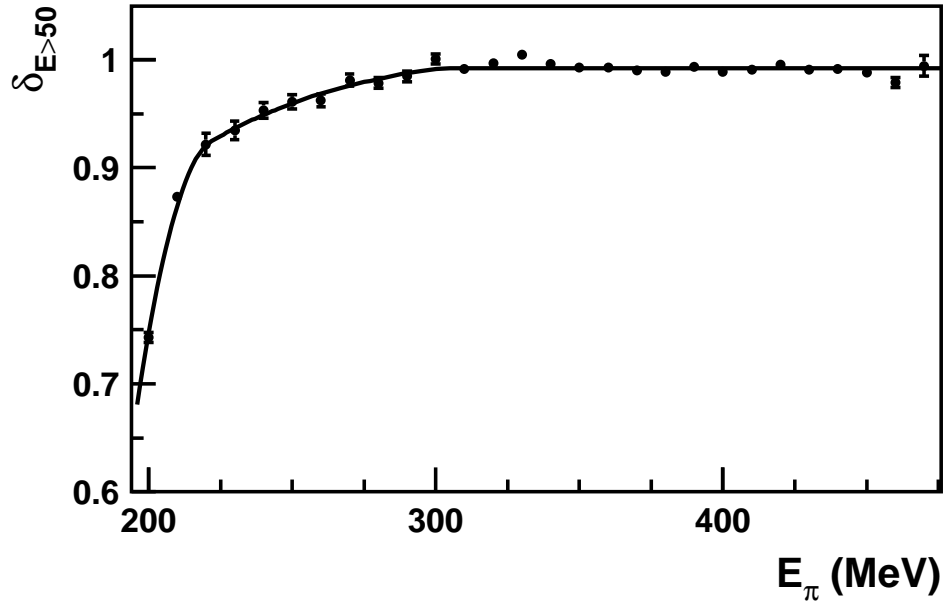


FIG. 15: The $\delta_{E>50}$ correction coefficient associated to the pions energy deposition cut in dependence on the pion energy E_{π} .

$\varepsilon_\pi \simeq 0.995$ for pions. In simulation these values actually do not differ from unity, while in reality the track finding probability for electrons is slightly greater than for pions. So the detection efficiency was multiplied by the correction coefficient:

$$\delta_{rec} = \left[\frac{\varepsilon_\pi}{\varepsilon_e} \right]^2 = 0,997 \quad (5)$$

Pions can be lost due to the nuclear interaction in the detector material before the tracking system, for example, via the reaction $\pi^\pm N \rightarrow \pi^\pm N$ with the final pion scattered at the large angle or via charge exchange reaction $\pi^\pm N \rightarrow \pi^0 N$. As a measure of systematic inaccuracy associated to this effect the difference from unity of the following quantity was used:

$$\delta_{nucl} = \left[\left(1 - \frac{n}{3N}\right) / \left(1 - \frac{m}{3M}\right) \right]^2, \quad (6)$$

where N and M is the pions numbers in experiment and simulation; n and m is the pions numbers in experiment and simulation which had a track in the drift chamber nearest to the beam-pipe, but the corresponding track in the second drift chamber and associated cluster in the calorimeter were not found. The particle loss probability was divided by 3 – the ratio of amounts of the matter between the drift chambers and before the tracking system. The deviation of δ_{nucl} from 1 was taken as a systematic error $\sigma_{nucl} = 0.2\%$.

Uncertainties in simulation of pions nuclear interactions imply that the cut on the particles energy deposition leads to an inaccuracy in detection efficiency of the $e^+e^- \rightarrow \pi^+\pi^-$ process. In order to take into account this inaccuracy, the detection efficiency was multiplied by the correction coefficients. The correction coefficients was obtained by using events of the $e^+e^- \rightarrow \pi^+\pi^-\pi^0$ reaction [30, 31, 32]. Pions energies in the $e^+e^- \rightarrow \pi^+\pi^-\pi^0$ events were determined via the kinematic fit. The pion energies were divided into the 10 MeV wide bins. For each bin the correction coefficient (Fig.15) was obtained:

$$\delta_{E>50} = \left[\frac{n_i/N_i}{m_i/M_i} \right]^2, \quad (7)$$

where i is the bin number, N_i and M_i are the pions numbers in experiment and simulation selected in the i th bin by the kinematic fit without any cut on the energy deposition in the calorimeter; n_i and m_i are the pions numbers in experiment and simulation under the condition that the pion energy deposition is greater than 50 MeV. To estimate systematic errors in determination of these correction coefficients, the ratio of the probability that both pions in simulated $e^+e^- \rightarrow \pi^+\pi^-$ events have energy deposition more than 50 MeV to the quantity $(m_i/M_i)^2$ was considered. This ratio is 0.994 at $\sqrt{s} > 420$ MeV and about 0.97 at $\sqrt{s} < 420$ MeV. The difference of this ratio from unity was taken as a systematic error $\sigma_{E>50}$ of the $\delta_{E>50}$ correction coefficient determination: $\sigma_{E>50} = 0.6\%$ at $\sqrt{s} > 420$ MeV and $\sigma_{E>50} = 3\%$ at $\sqrt{s} < 420$ MeV.

In the energy region $\sqrt{s} = 840 - 970$ MeV the probability to hit the muon/veto system for muons and pions varies from 1% upto 93%, and from 0.5% to 3% respectively. The usage of the muon system *veto* for events selection (*veto* = 0) leads to inaccuracy in the measured cross section determination due to the uncertainty in the simulation of the muons and pions traversing through the detector at $\sqrt{s} > 840$ MeV. In order to obtain the necessary corrections, the events close to the median plane $\phi < 10^\circ$, $170^\circ < \phi < 190^\circ$, $\phi > 350^\circ$, where the cosmic background is minimal, were used. The $e^+e^- \rightarrow \pi^+\pi^-$ cross section was measured with (*veto* = 0) and without (*veto* \geq 0) using the muon system, and the following correction coefficient was obtained for each energy point:

$$\delta_{veto} = \frac{\sigma(e^+e^- \rightarrow \pi^+\pi^-; veto \geq 0)}{\sigma(e^+e^- \rightarrow \pi^+\pi^-; veto = 0)} \quad (8)$$

It was found that $\delta_{veto} = 0.95$ at $\sqrt{s} = 970$ MeV and quickly rises up to 1 for lower energies.

The detection efficiencies of the processes $e^+e^- \rightarrow \pi^+\pi^-$, $\mu^+\mu^-$ and e^+e^- after all applied corrections are shown in Fig.16. The detection efficiency of the $e^+e^- \rightarrow e^+e^-$ reaction does not depend on energy, while for $e^+e^- \rightarrow \mu^+\mu^-$ and $\pi^+\pi^-$ processes it does. The decrease of the $e^+e^- \rightarrow \mu^+\mu^-$ process detection efficiency at $\sqrt{s} > 800$ MeV is caused by the fact that the probability for muons to hit the muon system rises with energy. The detection efficiency of the $e^+e^- \rightarrow \pi^+\pi^-$ process at $\sqrt{s} > 500$ MeV is determined mainly by the cuts on the pions angles. Below 500 MeV the detection efficiency decreases due to the cut on the pions energy deposition in the calorimeter. The statistical error $\leq 1\%$ of the detection efficiency determination was added to the cross section measurement error in each energy point. The total systematic error of the detection efficiency determination $\sigma_{eff} = \sigma_{E>50} \oplus \sigma_{nucl} \oplus \sigma_\theta$ is $\sigma_{eff} = 1\%$ at $\sqrt{s} \geq 420$ MeV and $\sigma_{eff} = 3.1\%$ at $\sqrt{s} < 420$ MeV.

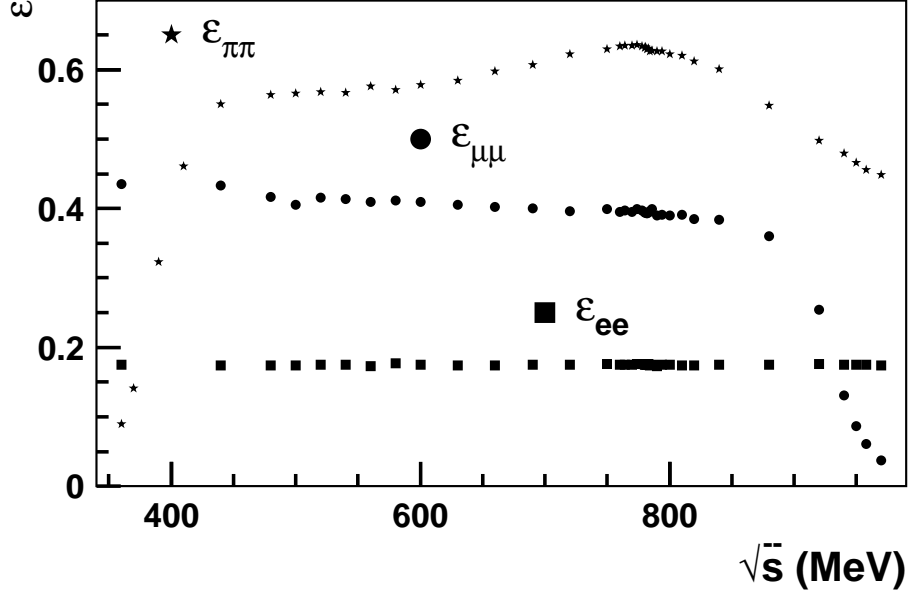


FIG. 16: The detection efficiencies $\varepsilon_{\pi\pi}$, ε_{ee} , $\varepsilon_{\mu\mu}$, of the $e^+e^- \rightarrow \pi^+\pi^-$, $\mu^+\mu^-$ and e^+e^- processes.

D. Measurement of the $e^+e^- \rightarrow \pi^+\pi^-$ cross section.

The number of selected events in the regions $R_{e/\pi} < 0.5$ and $R_{e/\pi} > 0.5$ are:

$$N = N_{\pi\pi} + N_{ee} + N_{\mu\mu} + N_{\mu} + N_{3\pi}, \quad (9)$$

$$M = M_{\pi\pi} + M_{ee} + M_{\mu\mu} + M_{\mu} + M_{3\pi}. \quad (10)$$

Here N and M are the events numbers in the regions $R_{e/\pi} < 0.5$ and $R_{e/\pi} > 0.5$ respectively. N_{μ} , M_{μ} and $N_{3\pi}$, $M_{3\pi}$ are the number of background events due to cosmic muons and the $e^+e^- \rightarrow \pi^+\pi^-\pi^0$ process, calculated as was described above. The $e^+e^- \rightarrow \mu^+\mu^-$ process events number can be written as:

$$N_{\mu\mu} = \sigma_{\mu\mu} \times \varepsilon_{\mu\mu} \times (1 - \epsilon_{\mu\mu}) \times IL, \quad (11)$$

$$M_{\mu\mu} = \sigma_{\mu\mu} \times \varepsilon_{\mu\mu} \times \epsilon_{\mu\mu} \times IL, \quad (12)$$

where $\sigma_{\mu\mu}$ is the $e^+e^- \rightarrow \mu^+\mu^-$ process cross section obtained according to Ref.[27], $\varepsilon_{\mu\mu}$ is the process detection efficiency, $\epsilon_{\mu\mu}$ is the probability for the $e^+e^- \rightarrow \mu^+\mu^-$ process events to have $R_{e/\pi} > 0.5$. IL is the integrated luminosity:

$$IL = \frac{M_{ee}}{\sigma_{ee} \times \varepsilon_{ee} \times \epsilon_{ee}}, \quad (13)$$

where ε_{ee} and ϵ_{ee} are the detection efficiency and the probability to have $R_{e/\pi} > 0.5$ for the process $e^+e^- \rightarrow e^+e^-$, σ_{ee} is the process cross section with the $30^\circ < \theta < 150^\circ$ angular cut for the electron and positron in the final state. The cross section σ_{ee} was calculated by using BHWIDE 1.04 [33] code with accuracy 0.5 %. The $e^+e^- \rightarrow \pi^+\pi^-$

process events number with $R_{e/\pi} > 0.5$ and the $e^+e^- \rightarrow e^+e^-$ process events number with $R_{e/\pi} < 0.5$ can be written in the following way:

$$N_{ee} = \frac{1 - \epsilon_{ee}}{\epsilon_{ee}} \times M_{ee} = \lambda_{ee} \times M_{ee}, \quad M_{\pi\pi} = \frac{1 - \epsilon_{ee}}{\epsilon_{ee}} \times N_{\pi\pi} = \lambda_{\pi\pi} \times N_{\pi\pi}.$$

The $e^+e^- \rightarrow e^+e^-$ process events number with $R_{e/\pi} > 0.5$ and the $e^+e^- \rightarrow \pi^+\pi^-$ process events number with $R_{e/\pi} < 0.5$ are equal to:

$$M_{ee} = \frac{M - M_\mu - \lambda_{\pi\pi} \times (N - N_\mu)}{\kappa - \Delta \times \lambda_{\pi\pi}}, \quad (14)$$

$$N_{\pi\pi} = N - N_\mu - M_{ee} \times \Delta. \quad (15)$$

Here

$$\Delta = \lambda_{ee} + \frac{\sigma_{\mu\mu} \times \varepsilon_{\mu\mu} \times (1 - \epsilon_{\mu\mu}) + N_{3\pi}/IL}{\sigma_{ee} \times \varepsilon_{ee} \times \epsilon_{ee}},$$

$$\kappa = 1 + \frac{\sigma_{\mu\mu} \times \varepsilon_{\mu\mu} \times \epsilon_{\mu\mu} + M_{3\pi}/IL}{\sigma_{ee} \times \varepsilon_{ee} \times \epsilon_{ee}}.$$

The percentage of each process in the selected events in dependence on energy \sqrt{s} is shown in Fig.17. The experimental angular distributions agree with the sum of distributions for each process weighted according to its contribution (Fig.18).

The $e^+e^- \rightarrow \pi^+\pi^-$ process cross section is calculated from the following formula:

$$\sigma_{\pi\pi} = \frac{N_{\pi\pi}}{IL \times \varepsilon_{\pi\pi} \times (1 - \epsilon_{\pi\pi})} = \frac{\sigma_{ee} \times \varepsilon_{ee} \times \epsilon_{ee}}{\varepsilon_{\pi\pi} \times (1 - \epsilon_{\pi\pi})} \times \left[\frac{\kappa - \Delta \times \lambda_{\pi\pi}}{\frac{M - M_\mu}{N - N_\mu} - \lambda_{\pi\pi}} - \Delta \right]. \quad (16)$$

In order to estimate the systematic uncertainty due to $e - \pi$ discrimination, the pseudo $\pi\pi$ and pseudo ee events in the experiment and simulation were formed. The pseudo $\pi\pi$ events were constructed by using pions from the $e^+e^- \rightarrow \pi^+\pi^-\pi^0$ reaction. In order to construct the pseudo $\pi\pi$ event with the pions having energy E_0 , two charged pions with energies E_π such that $|E_0 - E_\pi| < 10$ MeV were used from two separate $e^+e^- \rightarrow \pi^+\pi^-\pi^0$ events. Of course, such pseudo $\pi\pi$ events are in general not collinear but this is irrelevant for our purposes here. The pseudo ee event was constructed analogously from the particles of two separate collinear events such that their partners in these events have energy depositions in the calorimeter layers typical for electrons. Fig.19 and 20 show probabilities for the discrimination parameter to have values less than some magnitude in experiment and simulation for such pseudo events. Using these distributions, the corrections to the probabilities for the separation parameter $R_{e/\pi}$ to be greater or less than 0.5 was obtained. The difference between cross sections measured with and without these corrections was taken as a systematic error and its value does not exceed 0.5 % for different energy points.

The obtained cross sections together with the radiative corrections δ_{rad} , including the initial and final state radiation, are presented in Table I. The δ_{rad} radiative correction was calculated according to Ref.[28]. The accuracy of its determination is 0.2 %. Having at hand the radiative corrections the Born cross section for the $e^+e^- \rightarrow \pi^+\pi^-$ process can be extracted as follows

$$\sigma_0(s) = \frac{\sigma_{\pi\pi}(s)}{\delta_{rad}(s)} \quad (17)$$

The value of $\delta_{rad}(s)$ depends on the cross section at lower energies, so it was calculated iteratively. The iteration stops then its value changes by not more than 0.1 % in consecutive iterations. The form factor values

$$|F_\pi(s)|^2 = \frac{3s}{\pi\alpha^2\beta^3} \sigma_{\pi\pi}(s), \quad \beta = \sqrt{1 - 4m_\pi^2/s}$$

are also listed in Table I. To evaluate the value of $R(s) = \sigma(e^+e^- \rightarrow \text{hadrons})/\sigma(e^+e^- \rightarrow \mu^+\mu^-)$, which is used in dispersion integrals calculation, the bare cross section $e^+e^- \rightarrow \pi^+\pi^-$ is used (the cross section without vacuum polarization contribution but taking into account the final state radiation):

$$\sigma_{\pi\pi}^{pol}(s) = \sigma_0(s) \times |1 - \Pi(s)|^2 \times \left(1 + \frac{\alpha}{\pi} a(s) \right), \quad (18)$$

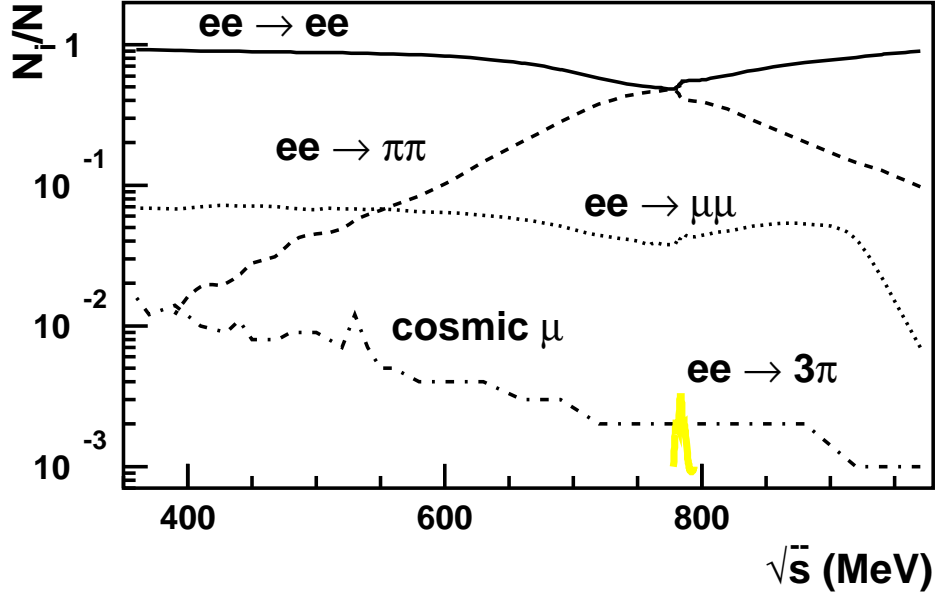


FIG. 17: The percentage of the $e^+e^- \rightarrow e^+e^-, \pi^+\pi^-, \mu^+\mu^-, \pi^+\pi^-\pi^0$ and cosmic background events in dependence on energy \sqrt{s}

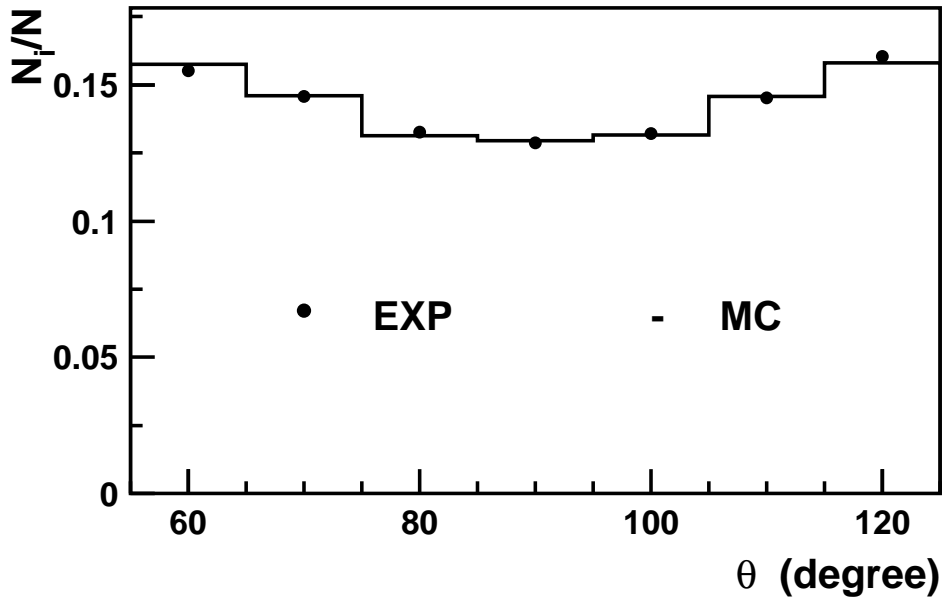


FIG. 18: The θ angle distributions of all collinear events at \sqrt{s} from 880 MeV to 630 MeV. Dots – experiment, histogram – simulation.

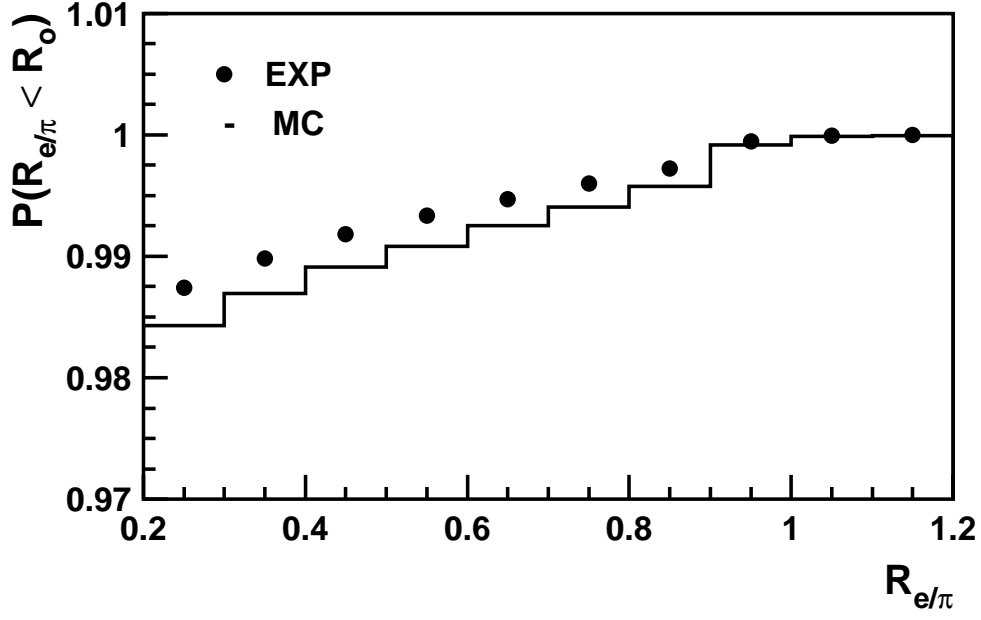


FIG. 19: The probability of the pseudo $\pi\pi$ events to have $R_{e/\pi}$ value less than some R_0 . Dots – experiment, histogram – simulation.

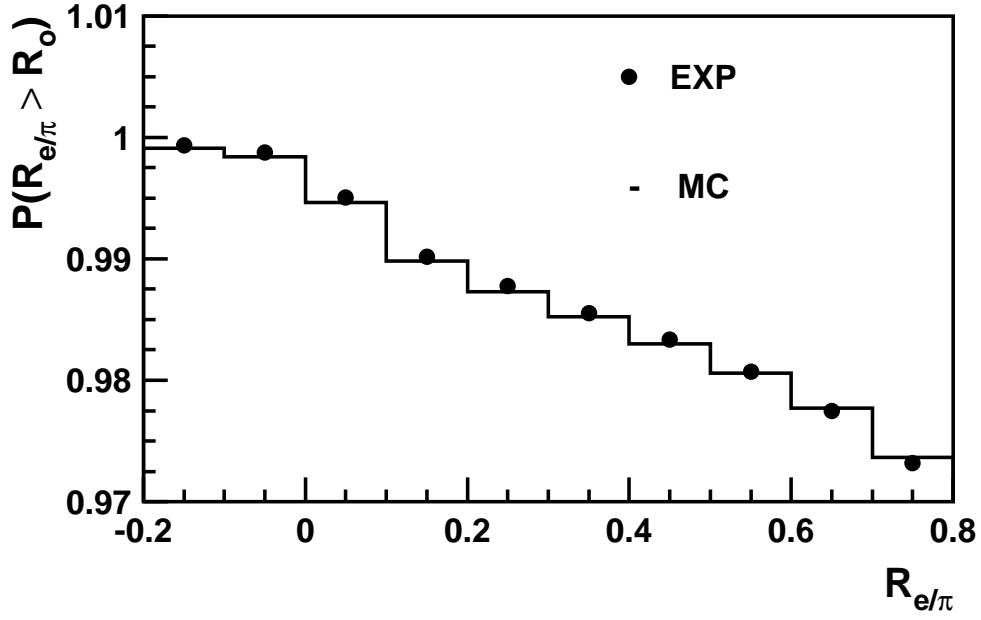


FIG. 20: The probability of the pseudo ee events to have $R_{e/\pi}$ value greater than some R_0 . Dots – experiment, histogram – simulation.

TABLE I: The results of the $e^+e^- \rightarrow \pi^+\pi^-$ cross section measurements. $\sigma_{\pi\pi}$ is the $e^+e^- \rightarrow \pi^+\pi^-$ cross section taking into account the radiative corrections due to the initial and final state radiation, δ_{rad} is the radiative correction due to the initial and final state radiation, σ_0 and $|F_\pi|^2$ are the cross section and the form factor of the $e^+e^- \rightarrow \pi^+\pi^-$ process after the radiative corrections were undressed, $\sigma_{\pi\pi}^{pol}$ is the $e^+e^- \rightarrow \pi^+\pi^-$ undressed cross section without vacuum polarization but with the final state radiation. Only uncorrelated errors are shown. The correlated systematic error σ_{sys} is 1.3 % for $\sqrt{s} \geq 420$ MeV and 3.2 % for $\sqrt{s} < 420$ MeV.

\sqrt{s} (MeV)	$\sigma_{\pi\pi}$ (nb)	δ_{rad}	σ_0 (nb)	$ F_\pi ^2$	$\sigma_{\pi\pi}^{pol}$ (nb)
970.	118.12± 2.76	1.491	79.20± 1.85	3.91± 0.09	77.53± 1.81
958.	137.16± 2.94	1.454	94.34± 2.02	4.56± 0.10	92.16± 1.97
950.	150.02± 2.85	1.430	104.88± 1.99	4.99± 0.09	102.35± 1.94
940.	166.55± 2.27	1.400	119.00± 1.62	5.56± 0.08	116.01± 1.58
920.	204.99± 7.14	1.340	152.96± 5.33	6.89± 0.24	148.60± 5.18
880.	310.82± 3.52	1.220	254.67± 2.88	10.65± 0.12	245.94± 2.78
840.	513.80± 4.76	1.106	464.48± 4.30	17.99± 0.17	446.64± 4.13
820.	676.03± 5.99	1.055	640.60± 5.68	23.86± 0.21	614.57± 5.45
810.	760.19± 6.58	1.032	736.34± 6.37	26.90± 0.23	704.79± 6.10
800.	856.66± 7.32	1.013	845.61± 7.23	30.28± 0.26	807.33± 6.90
794.	890.86± 7.43	1.009	883.09± 7.37	31.25± 0.26	838.38± 7.00
790.	892.35±17.70	1.015	879.09±17.44	30.86± 0.61	829.16± 16.45
786.	926.47± 7.84	1.031	898.19± 7.60	31.28± 0.26	842.92± 7.13
785.	941.34± 9.33	1.032	911.99± 9.04	31.70± 0.31	858.12± 8.51
784.	989.76±20.12	1.025	966.05±19.64	33.51± 0.68	915.22± 18.61
783.	1060.12±11.38	1.010	1050.08±11.27	36.35± 0.39	1005.99± 10.80
782.	1123.55±26.83	0.989	1136.34±27.14	39.26± 0.94	1102.62± 26.33
781.	1158.03±10.80	0.971	1192.83±11.12	41.13± 0.38	1169.48± 10.90
780.	1211.67± 9.98	0.957	1266.56±10.43	43.59± 0.36	1252.62± 10.32
778.	1273.38± 9.47	0.944	1349.27±10.03	46.25± 0.34	1343.80± 9.99
774.	1282.06± 9.49	0.938	1366.85±10.12	46.48± 0.34	1361.99± 10.08
770.	1249.25± 9.26	0.935	1336.51± 9.91	45.08± 0.33	1330.42± 9.86
764.	1247.24± 9.35	0.932	1338.62±10.04	44.61± 0.33	1331.35± 9.99
760.	1244.74± 9.58	0.927	1342.60±10.33	44.39± 0.34	1335.30± 10.27
750.	1219.07±21.50	0.920	1325.56±23.38	42.95± 0.76	1321.82± 23.31
720.	989.95± 6.62	0.910	1087.59± 7.27	33.15± 0.22	1091.88± 7.30
690.	717.99± 7.78	0.915	784.79± 8.50	22.50± 0.24	789.95± 8.56
660.	515.95± 5.87	0.923	558.83± 6.36	15.07± 0.17	561.19± 6.39
630.	382.69± 8.35	0.933	410.32± 8.95	10.41± 0.23	411.22± 8.97
600.	287.18±10.56	0.940	305.50±11.23	7.30± 0.27	305.61± 11.23
580.	255.24±14.39	0.945	270.24±15.24	6.22± 0.35	269.85± 15.22
560.	226.60±12.41	0.948	239.01±13.09	5.30± 0.29	238.63± 13.07
550.	217.52±17.51	0.950	228.99±18.43	4.99± 0.40	228.29± 18.37
540.	212.67±13.55	0.952	223.47±14.24	4.78± 0.30	222.82± 14.20
530.	200.04±22.75	0.953	210.00±23.88	4.42± 0.50	209.43± 23.82
520.	178.13±10.25	0.954	186.73±10.75	3.87± 0.22	186.26± 10.72
510.	174.28±16.65	0.954	182.60±17.45	3.73± 0.36	181.82± 17.38
500.	175.22±10.78	0.955	183.52±11.29	3.70± 0.23	182.77± 11.24
480.	165.18± 9.58	0.955	172.90±10.03	3.41± 0.20	172.29± 9.99
470.	143.94±13.21	0.955	150.71±13.83	2.94± 0.27	150.22± 13.78
450.	141.32±14.21	0.954	148.10±14.89	2.86± 0.29	147.42± 14.82
440.	116.15±15.58	0.953	121.86±16.35	2.35± 0.32	121.34± 16.28
430.	111.27±12.60	0.952	116.86±13.23	2.26± 0.26	116.41± 13.18
410.	127.38±19.11	0.949	134.23±20.14	2.64± 0.40	133.84± 20.08
390.	121.81±22.48	0.944	128.98±23.80	2.65± 0.49	128.76± 23.76

where $\Pi(s)$ is the polarization operator calculated according to the Ref.[27] from the known $e^+e^- \rightarrow$ hadrons cross section [34]. The last factor takes into account the final state radiation, and $a(s)$ has the form [35]

$$a(s) = \frac{1+\beta^2}{\beta} \left[4Li_2\left(\frac{1-\beta}{1+\beta}\right) + 2Li_2\left(-\frac{1-\beta}{1+\beta}\right) - 3\ln\frac{2}{1+\beta} \ln\frac{1+\beta}{1-\beta} - 2\ln\beta \ln\frac{1+\beta}{1-\beta} \right] -$$

TABLE II: Various contributions to the systematic error of the $e^+e^- \rightarrow \pi^+\pi^-$ cross section determination. σ_{sys} is the total systematic error, $\sigma_{eff} = \sigma_{E>50} \oplus \sigma_{nucl} \oplus \sigma_{\theta}$ is the systematic inaccuracy of the detection efficiency determination.

Error	Contribution at $\sqrt{s} \geq 420$ MeV	Contribution at $\sqrt{s} < 420$ MeV
$\sigma_{E>50}$	0.6 %	3.0 %
σ_{nucl}	0.2 %	0.2 %
σ_{θ}	0.8 %	0.8 %
σ_{eff}	1.0 %	3.1 %
σ_{sep}	0.5 %	0.5 %
σ_{IL}	0.5 %	0.5 %
σ_{rad}	0.2 %	0.2 %
σ_{sys}	1.3 %	3.2 %

$$-3 \ln \frac{4}{1-\beta^2} - 4 \ln \beta + \frac{1}{\beta^3} \left[\frac{5}{4} (1+\beta^2)^2 - 2 \right] \times \ln \frac{1+\beta}{1-\beta} + \frac{3}{2} \frac{1+\beta^2}{\beta^2}.$$

Here

$$Li_2(x) = - \int_0^x dt \ln(1-t)/t.$$

The values of $\sigma_{\pi\pi}^{pol}(s)$ are listed in Table I.

The total systematic error of the cross section determination is:

$$\sigma_{sys} = \sigma_{eff} \oplus \sigma_{sep} \oplus \sigma_{IL} \oplus \sigma_{rad}.$$

Here σ_{eff} is the systematic error of the detection efficiency determination, σ_{sep} is the systematic error associated with the $e - \pi$ separation, σ_{IL} is the systematic error of the integrated luminosity determination, and σ_{rad} is the uncertainty of the radiative correction calculation. The magnitudes of various contributions to the total systematic error are shown in Table II. The total systematic error of the cross section determinations is $\sigma_{sys} = 1.3$ % at $\sqrt{s} \geq 420$ MeV and $\sigma_{sys} = 3.2$ % at $\sqrt{s} < 420$ MeV.

IV. THE $e^+e^- \rightarrow \pi^+\pi^-$ CROSS SECTION ANALYSIS

A. Theoretical framework

In the framework of the vector meson dominance model, the cross section of the $e^+e^- \rightarrow \pi^+\pi^-$ process is

$$\sigma_{\pi\pi}(s) = \frac{4\pi\alpha^2}{s^{3/2}} P_{\pi\pi}(s) |A_{\pi\pi}(s)|^2 \quad (19)$$

Here $P_{\pi\pi}(s)$ is the phase space factor:

$$P_{\pi\pi}(s) = q_{\pi}^3(s), \quad q_{\pi}(s) = \frac{1}{2} \sqrt{s - 4m_{\pi}^2}.$$

Amplitudes of the $\gamma^* \rightarrow \pi^+\pi^-$ transition have the form:

$$|A_{\pi\pi}(s)|^2 = \left| \sqrt{\frac{3}{2}} \frac{1}{\alpha} \sum_{V=\rho,\omega,\rho',\rho''} \frac{\Gamma_V m_V^3 \sqrt{m_V \sigma(V \rightarrow \pi^+\pi^-)}}{D_V(s)} \frac{e^{i\phi_{\rho V}}}{\sqrt{q_{\pi}^3(m_V)}} \right|^2, \quad (20)$$

where

$$D_V(s) = m_V^2 - s - i\sqrt{s}\Gamma_V(s), \quad \Gamma_V(s) = \sum_f \Gamma(V \rightarrow f, s).$$

Here f denotes the final state of the V vector meson decay, m_V is the vector meson mass, $\Gamma_V = \Gamma_V(m_V)$. The following forms of the energy dependence of the vector mesons total widths were used:

$$\Gamma_\omega(s) = \frac{m_\omega^2}{s} \frac{q_\pi^3(s)}{q_\pi^3(m_\omega)} \Gamma_\omega B(\omega \rightarrow \pi^+ \pi^-) + \frac{q_{\pi\gamma}^3(s)}{q_{\pi\gamma}^3(m_\omega)} \Gamma_\omega B(\omega \rightarrow \pi^0 \gamma) + \frac{W_{\rho\pi}(s)}{W_{\rho\pi}(m_\omega)} \Gamma_\omega B(\omega \rightarrow 3\pi),$$

$$\Gamma_V(s) = \frac{m_V^2}{s} \frac{q_\pi^3(s)}{q_\pi^3(m_V)} \Gamma_V \quad (V = \rho, \rho', \rho'')$$

Here $q_{\pi\gamma} = (s - m_\pi^2)/2\sqrt{s}$, $W_{\rho\pi}(s)$ is the phase space factor for the $\rho\pi \rightarrow \pi^+ \pi^- \pi^0$ final state [30, 31, 32]. In the energy dependence of the ρ, ρ', ρ'' mesons widths only the $V \rightarrow \pi^+ \pi^-$ decays were taken into account. Such approach is justified in the energy region $\sqrt{s} < 1000$ MeV. Nowadays the ρ', ρ'' decays are rather poorly known and therefore the same approximation was used also for the fitting of the data above 1000 MeV. The ω -meson mass and width were taken from the SND measurements: $m_\omega = 782.79$ MeV, $\Gamma_\omega = 8.68$ MeV [31].

The relative decay probabilities were calculated as follows

$$B(V \rightarrow X) = \frac{\sigma(V \rightarrow X)}{\sigma(V)}, \quad \sigma(V) = \sum_X \sigma(V \rightarrow X), \quad \sigma(V \rightarrow X) = \frac{12\pi B(V \rightarrow e^+ e^-) B(V \rightarrow X)}{m_V^2}.$$

In the analysis presented here we have used $\sigma(\omega \rightarrow \pi^0 \gamma) = 155.8$ nb, $\sigma(\omega \rightarrow 3\pi) = 1615$ nb obtained in the SND experiments [31, 36].

The parameter $\phi_{\rho V}$ is the relative interference phase between the vector mesons V and ρ , so $\phi_{\rho\rho} = 0$. The phases $\phi_{\rho V}$ can deviate from 180° or 0° , and their values can be energy dependent due to mixing between vector mesons. The phases $\phi_{\rho\rho'}$ and $\phi_{\rho\rho''}$ were fixed at 180° and 0° , because these values are consistent with the existing experimental data for the $e^+ e^- \rightarrow \pi^+ \pi^-$ reaction.

Taking into account the $\rho - \omega$ mixing, the $\omega \rightarrow \pi^+ \pi^-$ and $\rho \rightarrow \pi^+ \pi^-$ transition amplitudes can be written in the following way [37, 38]

$$A_{\omega \rightarrow \pi^+ \pi^-} + A_{\rho \rightarrow \pi^+ \pi^-} = \frac{g_{\gamma\rho}^{(0)} g_{\rho\pi\pi}^{(0)}}{D_\rho(s)} \left[1 - \frac{g_{\gamma\omega}^{(0)}}{g_{\gamma\rho}^{(0)}} \varepsilon(s) \right] + \frac{g_{\gamma\omega}^{(0)} g_{\rho\pi\pi}^{(0)}}{D_\omega(s)} \left[\varepsilon(s) + \frac{g_{\omega\pi\pi}^{(0)}}{g_{\rho\pi\pi}^{(0)}} \right], \quad (21)$$

where

$$\varepsilon(s) = \frac{-\Pi_{\rho\omega}}{D_\omega(s) - D_\rho(s)}, \quad |g_{V\gamma}| = \left[\frac{3m_V^3 \Gamma_V B(V \rightarrow e^+ e^-)}{4\pi\alpha} \right]^{1/2}, \quad |g_{V\pi\pi}| = \left[\frac{6\pi m_V^2 \Gamma_V B(V \rightarrow \pi^+ \pi^-)}{q_\pi^3(m_V)} \right]^{1/2}.$$

The superscript (0) denotes the coupling constants of the bare, unmixed state. $\Pi_{\rho\omega}$ is the polarization operator of the $\rho - \omega$ mixing:

$$\Pi_{\rho\omega}(s) = \text{Re}(\Pi_{\rho\omega}(s)) + i \text{Im}(\Pi_{\rho\omega}(s)). \quad (22)$$

The $\text{Im}(\Pi_{\rho\omega}(s))$ can be written as

$$\text{Im}(\Pi_{\rho\omega}(s)) = \sqrt{s} \left\{ \frac{g_{\rho\pi\pi}^{(0)} g_{\omega\pi\pi}^{(0)} q_\pi^3(s)}{6\pi s} + \frac{g_{\rho\pi\gamma}^{(0)} g_{\omega\pi\gamma}^{(0)} q_{\pi\gamma}^3(s) + g_{\rho\eta\gamma}^{(0)} g_{\omega\eta\gamma}^{(0)} q_{\eta\gamma}^3(s)}{3} \right\}, \quad (23)$$

where

$$g_{VP\gamma} = \left[\frac{3\Gamma_V B(V \rightarrow P\gamma)}{q_{P\gamma}^3(m_V)} \right]^{1/2}.$$

We neglected the contributions to $\text{Im}(\Pi_{\rho\omega}(s))$ due to VP intermediate state ($V = \omega, \rho, P = \pi, \eta$). The $\text{Re}(\Pi_{\rho\omega}(s))$ can be represented as

$$\text{Re}(\Pi_{\rho\omega}(s)) = \text{Re}(\Pi_{\rho\omega}^\gamma(s)) + \text{Re}(\Pi_{\rho\omega}'(s)), \quad (24)$$

where

$$\text{Re}(\Pi_{\rho\omega}^\gamma(s)) = \frac{-4\pi g_{\rho\gamma}^{(0)} g_{\omega\gamma}^{(0)}}{s} \quad (25)$$

represents the one-photon contribution to the $\text{Re}(\Pi_{\rho\omega}(s))$. Let us assume that the energy dependence of the $\text{Re}(\Pi'_{\rho\omega}(s))$ is negligible, then it can be expressed by using the measured branching ratio

$$B(\omega \rightarrow \pi^+\pi^-) = \frac{\Gamma_\rho(m_\omega)}{\Gamma_\omega} \left| \varepsilon(m_\omega) + \frac{g_{\omega\pi\pi}^{(0)}}{g_{\rho\pi\pi}^{(0)}} \right|^2 \quad (26)$$

as follows

$$\begin{aligned} \text{Re}(\Pi'_{\rho\omega}) &= \frac{4\pi g_{\rho\gamma}^{(0)} g_{\omega\gamma}^{(0)}}{m_\omega^2} + \frac{g_{\omega\pi\pi}^{(0)}}{g_{\rho\pi\pi}^{(0)}} (m_\omega^2 - m_\rho^2) + \\ &+ \sqrt{\left[\frac{\Gamma_\omega B(\omega \rightarrow \pi^+\pi^-)}{\Gamma_\rho(m_\omega)} \left| D_\omega(m_\omega) - D_\rho(m_\omega) \right|^2 - \left[\frac{g_{\rho\pi\gamma}^{(0)} g_{\omega\pi\gamma}^{(0)} q_{\pi\gamma}^3(m_\omega) + g_{\rho\eta\gamma}^{(0)} g_{\omega\eta\gamma}^{(0)} q_{\eta\gamma}^3(m_\omega)}{3} + \frac{g_{\omega\pi\pi}^{(0)}}{g_{\rho\pi\pi}^{(0)}} m_\omega \Gamma_\omega \right]^2} \end{aligned} \quad (27)$$

Equation (21) can be rewritten as follows

$$A_{\omega \rightarrow \pi^+\pi^-} + A_{\rho \rightarrow \pi^+\pi^-} = \sqrt{\frac{3}{2}} \frac{1}{\alpha} \sum_{V=\omega,\rho} \frac{\Gamma_V m_V^3 \sqrt{m_V \sigma(V \rightarrow \pi^+\pi^-)}}{D_V(s)} \frac{f_{V\pi\pi}(s)}{\sqrt{q_\pi(m_V)}}, \quad (28)$$

where

$$f_{V\pi\pi}(s) = \frac{r_{V\pi\pi}(s)}{r_{V\pi\pi}(m_V)},$$

and

$$r_{\rho\pi\pi}(s) = 1 - \frac{g_{\gamma\omega}^{(0)}}{g_{\gamma\rho}^{(0)}} \varepsilon(s), \quad r_{\omega\pi\pi}(s) = \varepsilon(s) + \frac{g_{\omega\pi\pi}^{(0)}}{g_{\rho\pi\pi}^{(0)}}$$

The theoretical value of the phase $\phi_{\rho\omega}$ can be calculated from the above given expressions: $\phi_{\rho\omega} = \arg(f_{\omega\pi\pi}(m_\omega)) - \arg(f_{\rho\pi\pi}(m_\rho)) \simeq 101^\circ$. The phase $\phi_{\rho\omega}$ almost does not depend on energy. In this calculation we assumed that the $\omega \rightarrow \pi^+\pi^-$ transition proceeds only via the $\rho - \omega$ mixing, that is $g_{\omega\pi\pi}^{(0)} = 0$. In order to determine the $g_{\rho\pi\pi}^{(0)}$, $g_{\gamma V}^{(0)}$ and $g_{VP\gamma}^{(0)}$ coupling constants, the corresponding measured decay widths were used.

B. Fit to the experimental data

The ρ' and ρ'' parameters were determined from the fit to the $e^+e^- \rightarrow \pi^+\pi^-$ cross section measured at the energy region $\sqrt{s} < 2400$ MeV by OLYA and DM2 detectors [17, 39], together with the isovector part of the $e^+e^- \rightarrow \pi^+\pi^-$ cross section calculated by assuming the CVC hypothesis from the spectral function of the $\tau^- \rightarrow \pi^-\pi^0\nu_\tau$ decay measured by CLEO II [5]:

$$\sigma_{\pi\pi}(m_i) = \frac{4(\pi\alpha)^2 B(\tau \rightarrow \pi\pi^0\nu_\tau)}{m_i} \frac{m_\tau^8}{B(\tau \rightarrow e\bar{\nu}_e\nu_\tau)} \frac{1}{12\pi|V_{ud}|^2 S_{EW}} \frac{1}{m_i(m_\tau^2 - m_i^2)^2(m_\tau^2 + 2m_i^2)} \frac{1}{N} \frac{N_i}{\Delta m_i}, \quad (29)$$

where m_i is the central value of the $\pi^-\pi^0$ pair invariant mass for the i -th bin, Δm_i is the bin width, N_i is the number of entries in the i -th bin, N is the total number of entries, $|V_{ud}|$ is the CKM matrix element, $S_{EW} = 1.0194$ is the radiative correction [3, 5, 40].

The obtained ρ' and ρ'' parameters were used in the fitting to the SND data (Table III, Fig.21). The free parameters of the fit were m_ρ , Γ_ρ , $\sigma(\rho \rightarrow \pi^+\pi^-)$, $\sigma(\omega \rightarrow \pi^+\pi^-)$, $\phi_{\rho\omega}$ and $\sigma(\rho' \rightarrow \pi^+\pi^-)$. The first fit was performed with $\sigma(\rho'' \rightarrow \pi^+\pi^-)$, ρ' and ρ'' masses and widths fixed at the values obtained from the fit to the CLEO II and DM2 data. The second and third fits were done without the ρ'' meson. The ρ' mass and width were fixed by using results of the fit to the CLEO II and DM2 data (the second variant in the Table III) and to the OLYA data (the third variant in the Table III). The values of the ρ and ω parameters exhibit a rather weak model dependence.

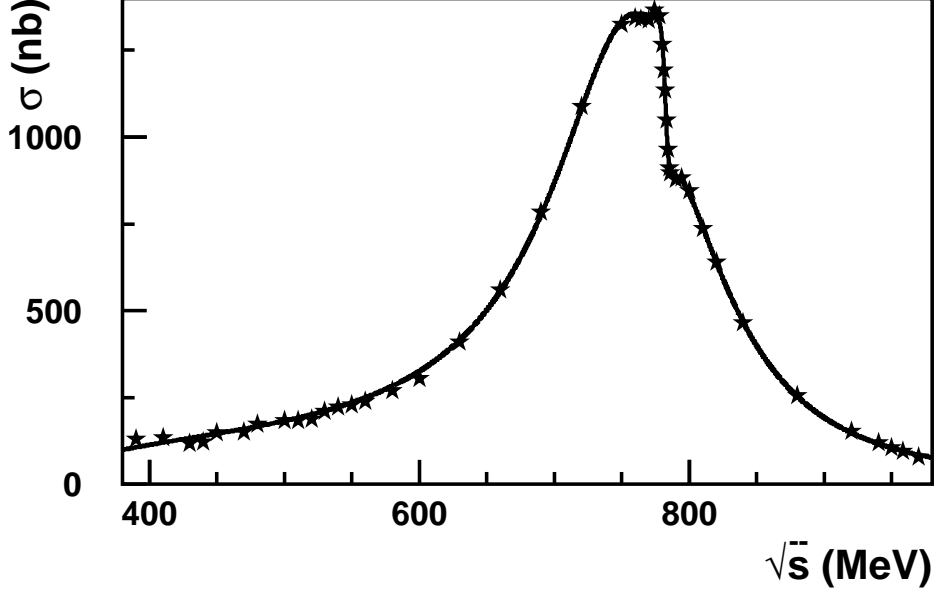


FIG. 21: The $e^+e^- \rightarrow \pi^+\pi^-$ cross section. Stars are the SND data obtained in this work, curve is the fit result.

TABLE III: Fit results. The column number N corresponds to the different variants of choice of the ρ' and ρ'' parameters.

N	1	2	3
m_ρ, MeV	774.9 ± 0.4	774.9 ± 0.4	774.9 ± 0.4
Γ_ρ, MeV	146.2 ± 0.8	146.4 ± 0.8	146.3 ± 0.8
$\sigma(\rho \rightarrow \pi^+\pi^-), \text{nb}$	1222 ± 7	1218 ± 7	1219 ± 7
$\sigma(\omega \rightarrow \pi^+\pi^-), \text{nb}$	30.2 ± 1.4	30.3 ± 1.4	30.3 ± 1.4
$\phi_{\rho\omega}, \text{degree}$	113.6 ± 1.3	113.4 ± 1.3	113.5 ± 1.3
$m_{\rho'}, \text{MeV}$	1403	1403	1360
$\Gamma_{\rho'}, \text{MeV}$	455	455	430
$\sigma(\rho' \rightarrow \pi^+\pi^-), \text{nb}$	3.8 ± 0.3	1.8 ± 0.2	1.9 ± 0.2
$m_{\rho''}, \text{MeV}$	1756		
$\Gamma_{\rho''}, \text{MeV}$	245		
$\sigma(\rho'' \rightarrow \pi^+\pi^-), \text{nb}$	1.7		
χ^2/N_{df}	50.2/39	48.8/39	49.4/39

V. DISCUSSION.

The comparison of the $e^+e^- \rightarrow \pi^+\pi^-$ cross section obtained in SND experiment with other results [8, 9, 17, 18, 19] is shown in Fig.22,23,24 and 25. In the energy region $\sqrt{s} < 600$ MeV all experimental data are in agreement (Fig.22). Above 600 MeV the OSPK(ORSAY-ACO)[8] and DM1 [9] points lay about 10 % lower than the SND ones (Fig.23). The SND cross section exceeds the OLYA and CMD measurements [17] by 6 ± 1 % in this energy region (Fig.24). The systematic error of OLYA measurement is 4 % and the OLYA data agree with the SND result. The systematic uncertainty of CMD result is 2 %, so the difference between the SND and CMD results is about 2.5 of joint systematic error. At the same time the SND and CMD data below 600 MeV agree well (Fig.22). The average deviation between CMD2 [18] and SND data is 1.4 ± 0.5 %, the systematic inaccuracies of these measurements are 0.6 % and 1.3

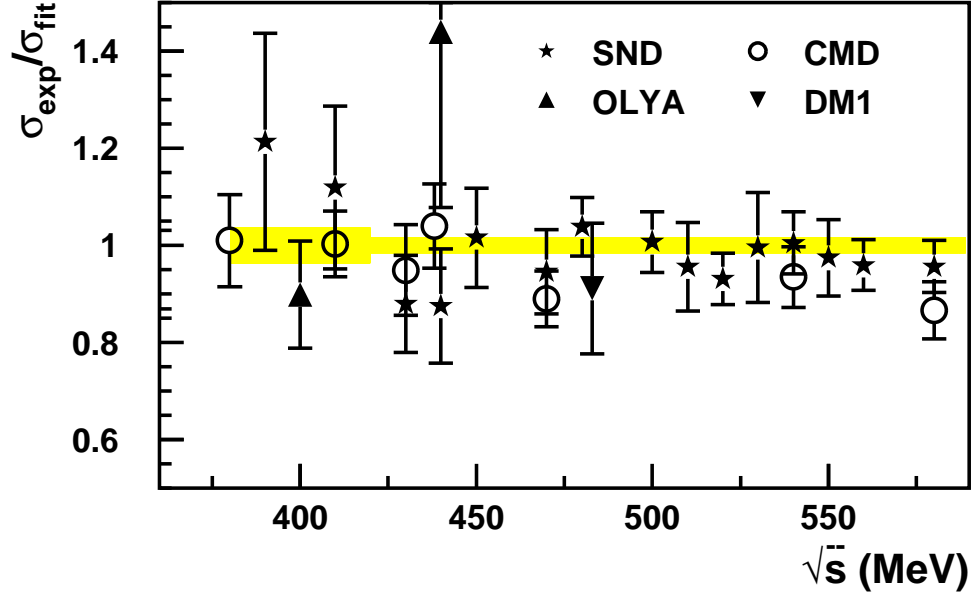


FIG. 22: The ratio of the $e^+e^- \rightarrow \pi^+\pi^-$ cross section obtained in different experiments to the fit curve (Fig.21). The shaded area shows the systematic error of the SND measurements. The SND (this work), CMD, OLYA and DM1 [9, 17] results are presented.

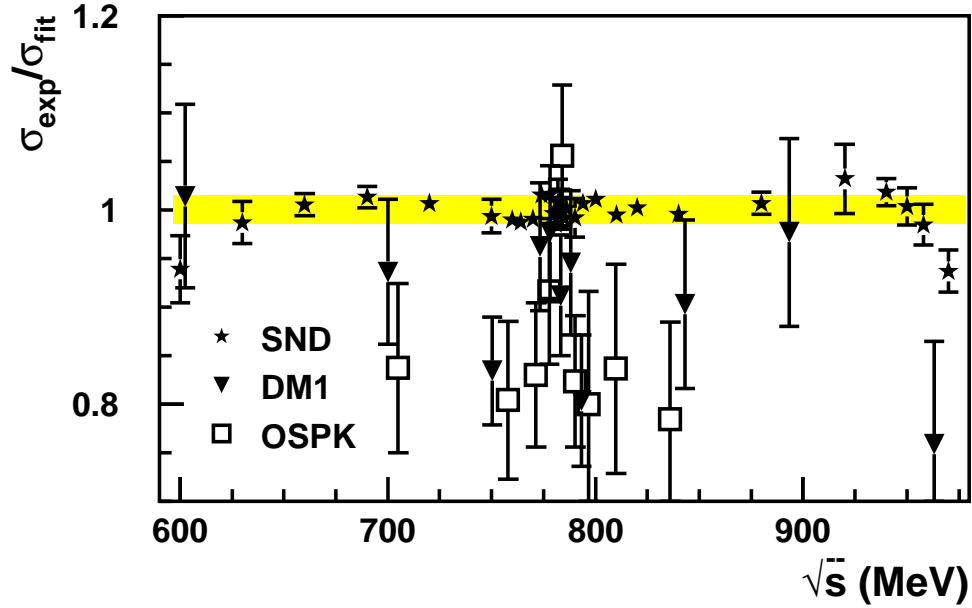


FIG. 23: The ratio of the $e^+e^- \rightarrow \pi^+\pi^-$ cross section obtained in different experiments to the fit curve (Fig.21). The shaded area shows the systematic error of the SND measurements. The SND (this work), DM1, OSPK [8, 9] results are presented.

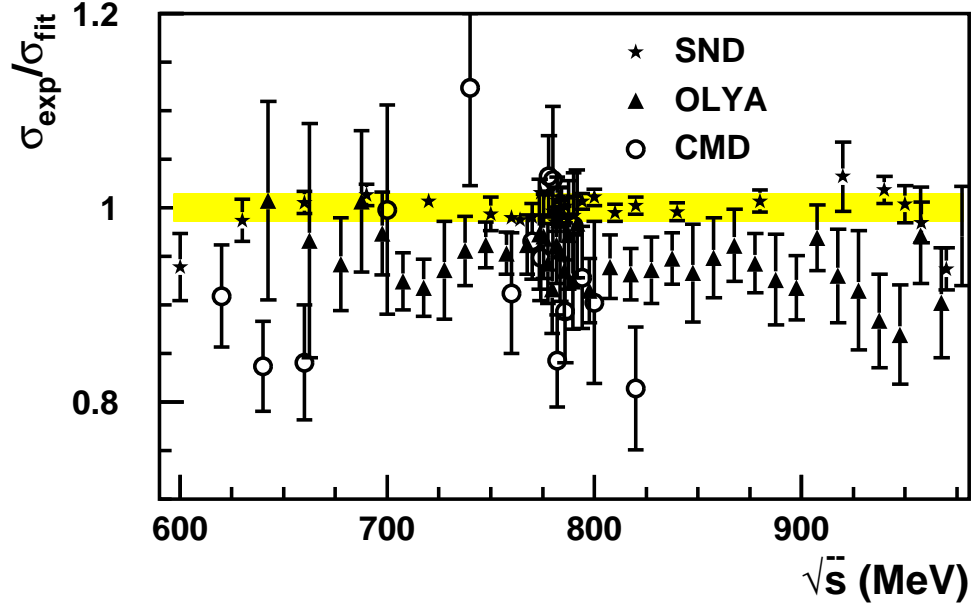


FIG. 24: The ratio of the $e^+e^- \rightarrow \pi^+\pi^-$ cross section obtained in different experiments to the fit curve (Fig.21). The shaded area shows the systematic error of the SND measurements. The SND (this work), OLYA and CMD [17] results are presented.

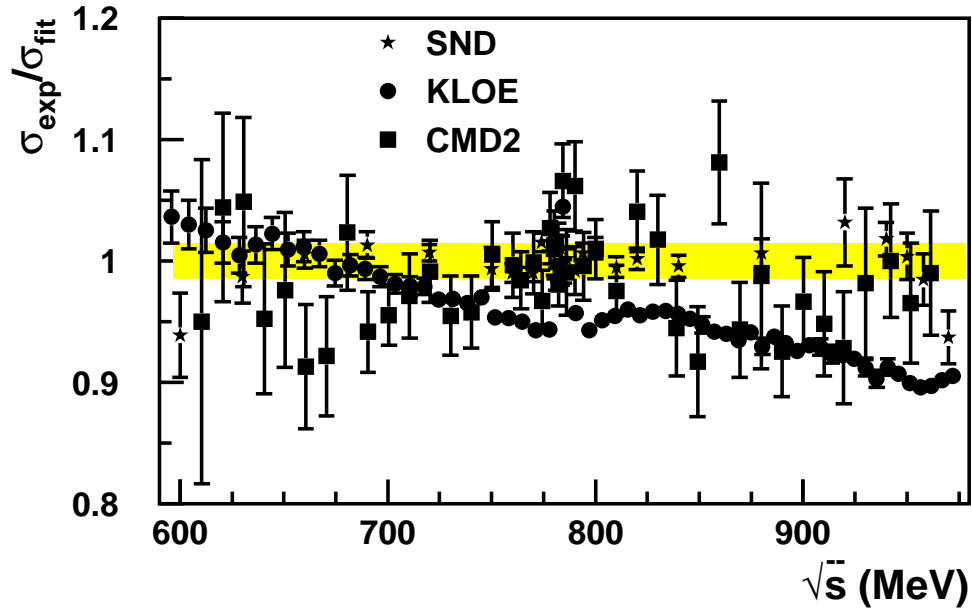


FIG. 25: The ratio of the $e^+e^- \rightarrow \pi^+\pi^-$ cross section obtained in different experiments to the fit curve (Fig.21). The shaded area shows the systematic error of the SND measurements. The SND (this work), CMD2 and KLOE [18, 19] results are presented.

% respectively. In the KLOE experiment at ϕ -factory DAFΦNE the form factor $|F_\pi(s)|^2$ was measured by using “radiative return” method with systematic error of 0.9 % [19]. In Ref.[19] the bare form factor is listed. So in order to compare the KLOE result with the SND one, the form factor was appropriately dressed by us. The results of this comparison are shown in Fig.25. The KLOE measurement is in conflict with the SND result as well as with the CMD2 one.

The ρ -meson parameters m_ρ , Γ_ρ , $\sigma(\rho \rightarrow \pi^+\pi^-)$ were determined from study of the $e^+e^- \rightarrow \pi^+\pi^-$ cross section. The ρ meson mass and width were found to be

$$m_\rho = 774.9 \pm 0.04 \pm 0.05 \text{ MeV},$$

$$\Gamma_\rho = 146.5 \pm 0.8 \pm 1.5 \text{ MeV}.$$

The systematic errors is related to the accuracy of the collider energy determination, to the model uncertainty and to the error of the cross section determination. The ρ -meson parameters were studied in other e^+e^- experiments by using the processes $e^+e^- \rightarrow \pi^+\pi^-$ [17, 18], $e^+e^- \rightarrow \rho\pi \rightarrow \pi^+\pi^-\pi^0$ [32, 41] and the $\tau^- \rightarrow \pi^-\pi^0\nu_\tau$ decay [3, 5]. The SND results are in agreement with these measurements as is shown in Fig.26 and 27.

The parameter $\sigma(\rho \rightarrow \pi^+\pi^-)$ was found to be

$$\sigma(\rho \rightarrow \pi^+\pi^-) = 1220 \pm 7 \pm 16 \text{ nb},$$

which corresponds to

$$B(\rho \rightarrow e^+e^-) \times B(\rho \rightarrow \pi^+\pi^-) = (4.991 \pm 0.028 \pm 0.066) \times 10^{-5},$$

$$\Gamma(\rho \rightarrow e^+e^-) = 7.31 \pm 0.021 \pm 0.11 \text{ keV}.$$

The systematic error includes the systematic uncertainties in the cross section measurement and the model dependence. A comparison of the $\Gamma(\rho \rightarrow e^+e^-)$ obtained in this work with other experimental results [8, 17, 18] and with the PDG world average [42] is shown in Fig.28. The SND result exceeds all previous measurements. It differs by about 1.5 standard deviations from the CMD2 measurement [18] and by 2 standard deviations from the PDG world average [42]. The difference of the ρ -meson leptonic widths obtained by SND and CMD2 should be attributed mainly to the difference in the total widths of the ρ -meson rather than to the difference in the cross section values. The value $\sigma(\rho \rightarrow \pi^+\pi^-) = 1198 \text{ nb}$, which can be obtained by using CMD2 cross section data reported in Ref.[18], agrees with the SND result within the measurements errors.

The parameter $\sigma(\omega \rightarrow \pi^+\pi^-)$ was found to be

$$\sigma(\omega \rightarrow \pi^+\pi^-) = 29.9 \pm 1.2 \pm 1.0 \text{ nb},$$

which corresponds to

$$B(\omega \rightarrow e^+e^-) \times B(\omega \rightarrow \pi^+\pi^-) = (1.247 \pm 0.062 \pm 0.042) \times 10^{-6}.$$

The systematic error is related to the model dependence, to the error of the cross section determination and to the accuracy of the collider energy determination. In the previous studies of the $e^+e^- \rightarrow \pi^+\pi^-$ reaction the relative probability of the $\omega \rightarrow \pi^+\pi^-$ decay was also reported. The comparison of $B(\omega \rightarrow \pi^+\pi^-) = 0.0175 \pm 0.0011$ obtained by using the SND data and the PDG value of the $\omega \rightarrow e^+e^-$ decay width [42] with the results of other experiments is shown in Fig.29. The SND result is the most precise.

The phase $\phi_{\rho\omega}$ was found to be

$$\phi_{\rho\omega} = 113.5 \pm 1.3 \pm 1.7 \text{ degree}.$$

This value differs by 6 standard deviations from 101° expected under assumption that the $\omega \rightarrow \pi^+\pi^-$ transition proceeds through the $\rho - \omega$ mixing mechanism. If instead of the phase $\phi_{\rho\omega}$, the ratio $\frac{g_{\omega\pi\pi}^{(0)}}{g_{\rho\pi\pi}^{(0)}}$ is the free parameter of the fit it follows that

$$\frac{g_{\omega\pi\pi}^{(0)}}{g_{\rho\pi\pi}^{(0)}} = 0.11 \pm 0.01.$$

This ratio corresponds to the too large direct transition width $\Gamma^{(0)}(\omega \rightarrow \pi^+\pi^-) = 1.82 \pm 0.33 \text{ MeV}$, while the natural expectation is $\Gamma^{(0)}(\omega \rightarrow \pi^+\pi^-) \approx \alpha^2\Gamma_\rho \approx 8 \text{ keV}$. Let us note, that the analysis of the OLYA and CMD2 data [17, 18]

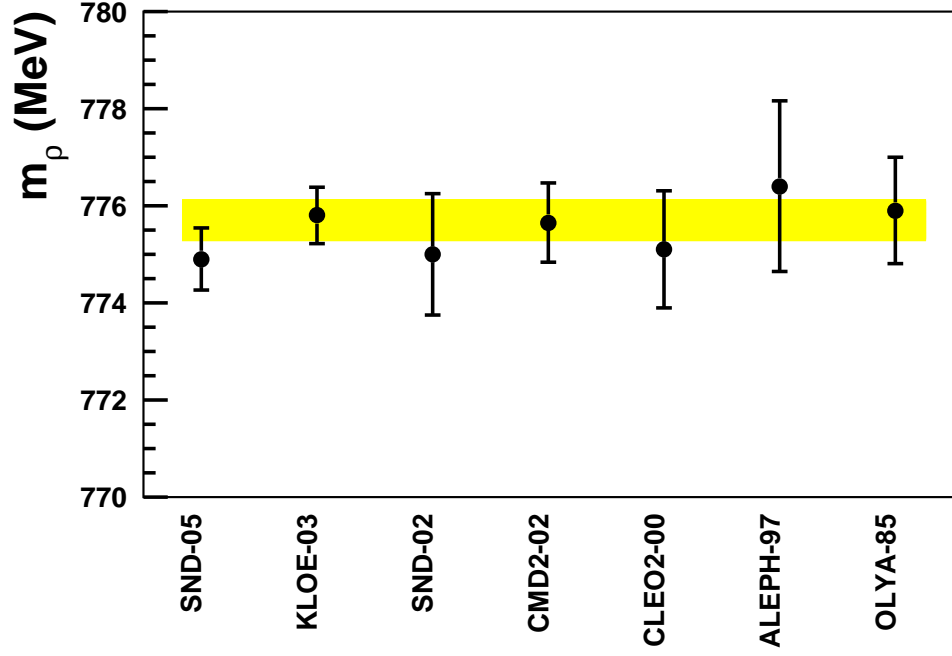


FIG. 26: The ρ -meson mass m_ρ measured in this work (SND-05) and in Ref.[3, 5, 17, 18, 32, 41]. The shaded area shows the average of the previous results.

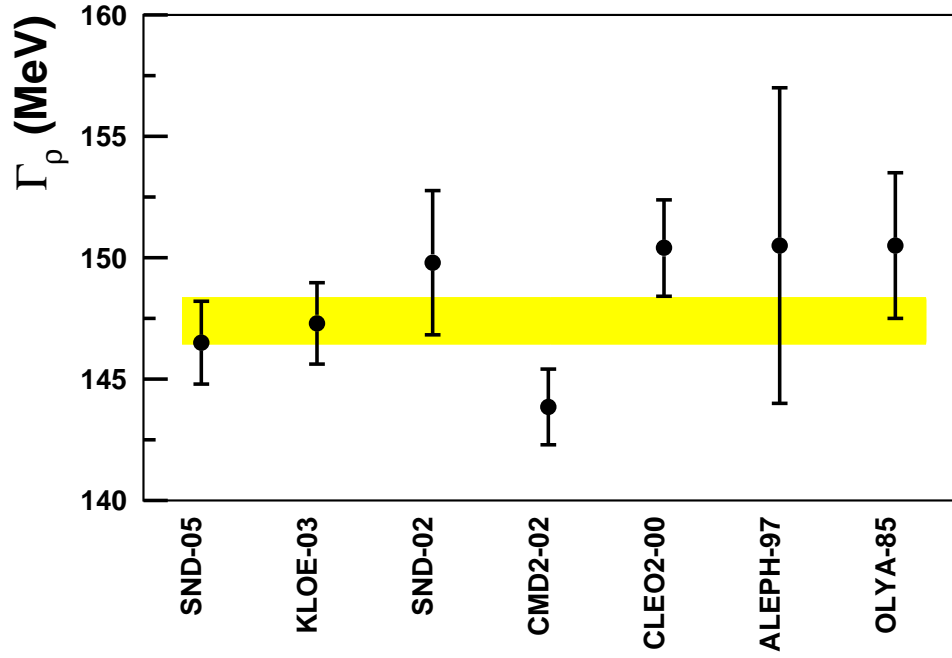


FIG. 27: The ρ meson width Γ_ρ measured in this work (SND-05) and in Ref.[3, 5, 17, 18, 32, 41]. The shaded area shows the average of the previous results.

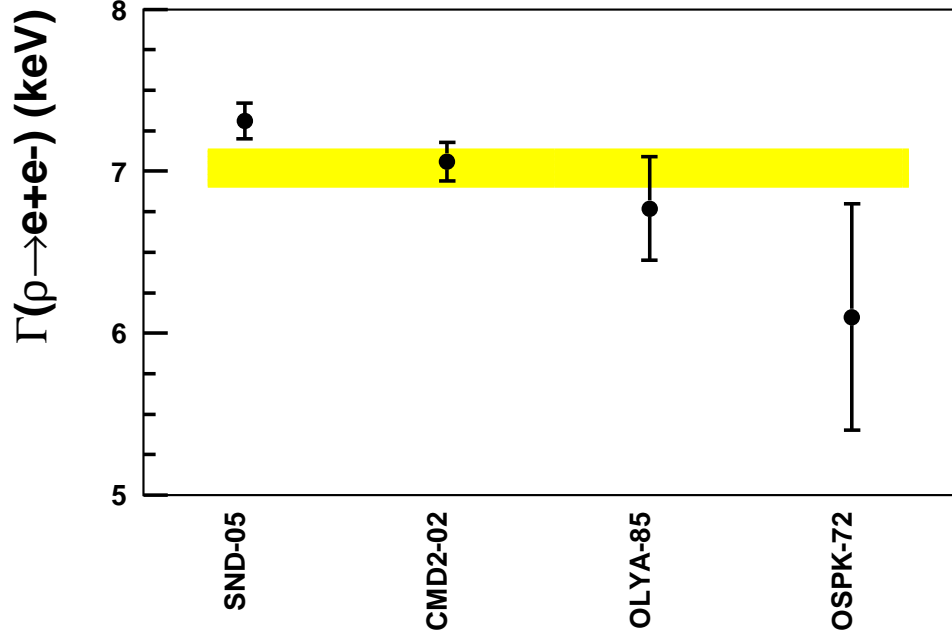


FIG. 28: The value of $\Gamma(\rho \rightarrow e^+e^-)$ obtained in this work (SND-05) and in Ref.[8, 17, 18]. The shaded area shows the world average value [42].

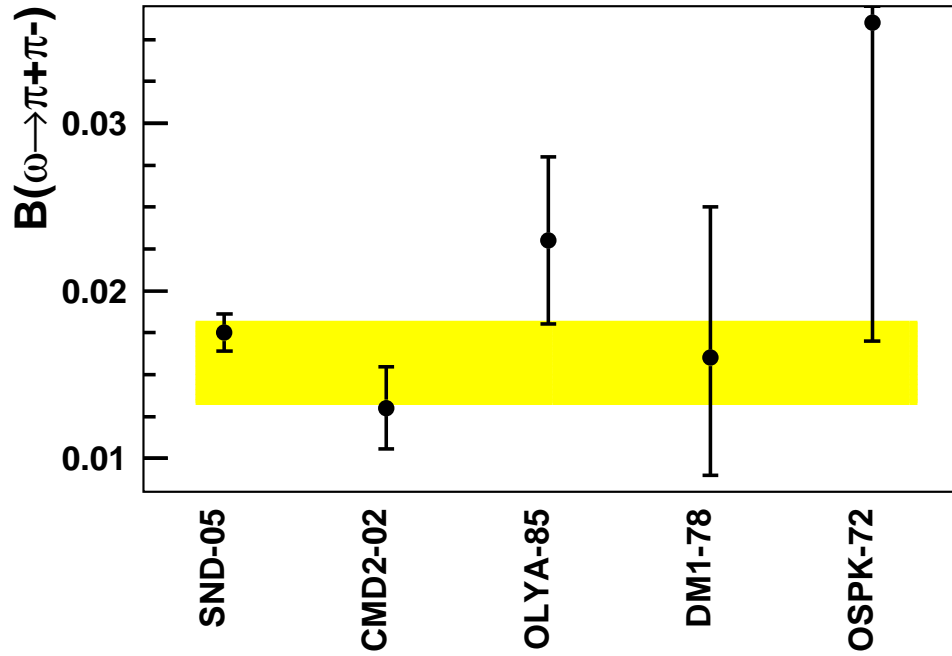


FIG. 29: The value of $B(\omega \rightarrow \pi^+\pi^-)$ obtained in this work (SND-05) and in Ref.[8, 9, 17, 18]. The shaded area shows the world average value [42].

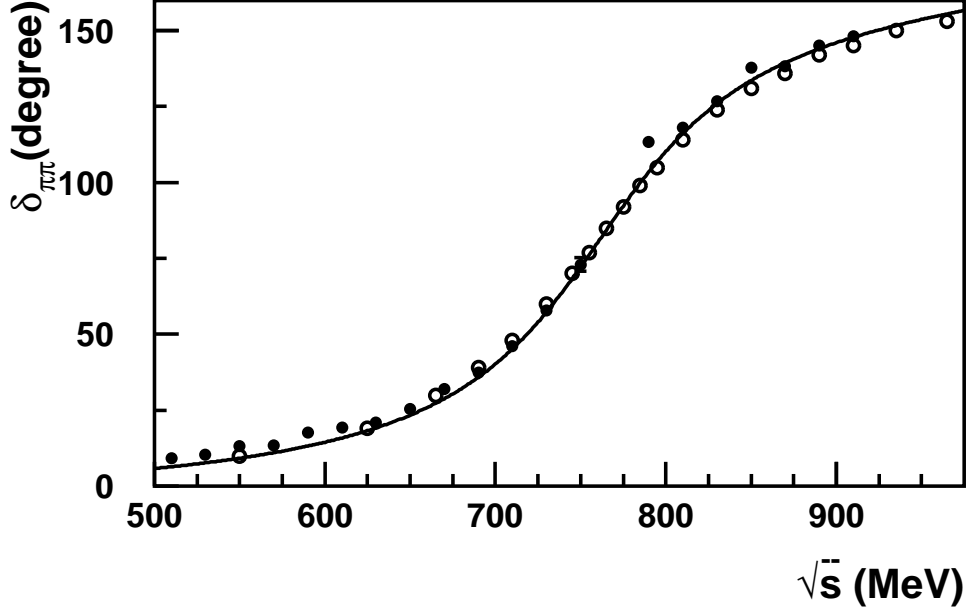


FIG. 30: The $\pi\pi$ scattering phase in the P-wave. Dots and circles are results of the phase measurements in Ref. [43, 44] by using the reaction $\pi N \rightarrow \pi\pi N$. The curve is the phase of the amplitude $A_{\rho \rightarrow \pi\pi} + A_{\rho \rightarrow \pi^+\pi^-}$ obtained from the fit to the SND data presented in this work.

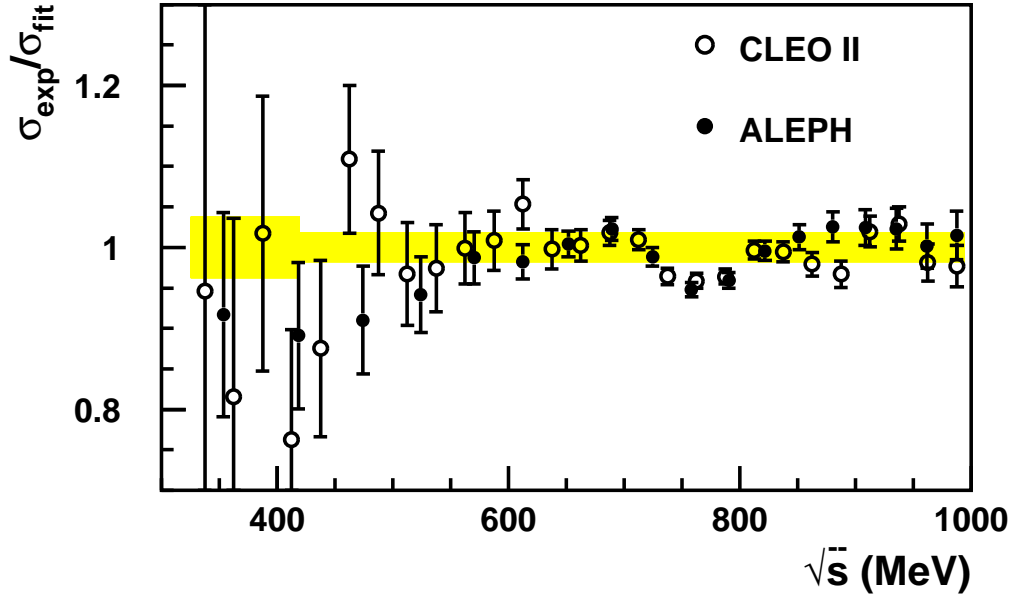


FIG. 31: The ratio of the $e^+e^- \rightarrow \pi^+\pi^-$ cross section calculated from the $\tau^- \rightarrow \pi^-\pi^0\nu_\tau$ decay spectral function measured in Ref.[3, 5] to the isovector part of the $e^+e^- \rightarrow \pi^+\pi^-$ cross section measured in this work. The shaded area shows the joint systematic error.

give the similar values of the $\phi_{\rho\omega}$ phase. This result can point out that the considerable direct transition $\omega \rightarrow \pi^+\pi^-$ exists. On the other hand this discrepancy can be attributed also to inadequacies of the applied theoretical model.

The comparison of the phase $\arg(A_{\rho \rightarrow \pi^+\pi^-} + A_{\rho' \rightarrow \pi^+\pi^-})$ with the $\pi\pi$ scattering phase in the P-wave [43, 44] is shown in Fig.30. These phases must be equal in the purely elastic scattering region. The agreement is satisfactory, in any case in the energy region $\sqrt{s} \approx m_\rho$ no essential difference is observed.

The comparison of the $e^+e^- \rightarrow \pi^+\pi^-$ cross section, obtained under the CVC hypothesis from the τ spectral function of the $\tau^- \rightarrow \pi^- \pi^0 \nu_\tau$ decay [3, 5] with isovector part of the cross section measured in this work is shown in Fig.31. The cross section obtained by SND was undressed from the vacuum polarization and the contribution from the $\omega \rightarrow \pi^+\pi^-$ decay was excluded. The cross section calculated from the τ spectral function was multiplied by the coefficient which takes into account the difference of the π^\pm and π^0 masses:

$$\delta = \left(\frac{q_\pi(s)}{q_{\pi^\pm}(s)} \right)^3 \frac{|A_{\pi^+\pi^-}(s)|^2}{|A_{\pi^0\pi^\pm}(s)|^2}, \quad q_{\pi^\pm}(s) = \frac{1}{2\sqrt{s}} [(s - (m_{\pi^0} + m_{\pi^\pm})^2)(s - (m_{\pi^0} - m_{\pi^\pm})^2)]^{1/2}.$$

The average deviation of the SND and τ data is about 1.5 %. For almost all energy points this deviation is within the joint systematic error $\simeq 1.6\%$. The 10% difference between e^+e^- and τ data at $\sqrt{s} > 800$ MeV, which was claimed in Ref.[45], is absent.

Using the $\sigma_{\pi\pi}^{pol}(s)$ cross section (Table I), the contribution to the anomalous magnetic moment of the muon, due to the $\pi^+\pi^-(\gamma)$ intermediate state in the vacuum polarization, was calculated via the dispersion integral:

$$a_\mu(\pi\pi, 390\text{MeV} \leq \sqrt{s} \leq 970\text{MeV}) = \left(\frac{\alpha m_\mu}{3\pi} \right)^2 \int_{s_{min}}^{s_{max}} \frac{R(s)K(s)}{s^2} ds,$$

where $s_{max} = 970$ MeV, $s_{min} = 390$ MeV, $K(s)$ is the known kernel and

$$R(s) = \frac{\sigma_{\pi\pi}^{pol}}{\sigma(e^+e^- \rightarrow \mu^+\mu^-)}, \quad \sigma(e^+e^- \rightarrow \mu^+\mu^-) = \frac{4\pi\alpha^2}{3s}.$$

The integral was evaluated by using the trapezoidal rule. To take into account the numerical integration errors, the correction method suggested in Ref.[46] was applied. As a result we obtained

$$a_\mu(\pi\pi, 390\text{MeV} \leq \sqrt{s} \leq 970\text{MeV}) = (488.7 \pm 2.6 \pm 6.6) \times 10^{-10}.$$

This is about 70 % of the total hadronic contribution to the anomalous magnetic moment of the muon $(g-2)/2$.

If the integration is performed for the energy region corresponding to the CMD2 measurements [18], then the result is $a_\mu(\pi\pi) = (385.6 \pm 5.2) \times 10^{-10}$, which is 1.8 % (1 standard deviation) higher than the CMD2 result: $a_\mu(\pi\pi) = (378, 6 \pm 3.5) \times 10^{-10}$. So no considerable difference between the SND and CMD2 results is observed.

VI. CONCLUSION

The cross section of the process $e^+e^- \rightarrow \pi^+\pi^-$ was measured in the SND experiment at the VEPP-2M collider in the energy region $390 < \sqrt{s} < 980$ MeV with accuracy 1.3 % at $\sqrt{s} \geq 420$ MeV and 3.4 % at $\sqrt{s} < 420$ MeV. The measured cross section was analyzed in the framework of the generalized vector meson dominance model. The following ρ -meson parameters were obtained: $m_\rho = 774.9 \pm 0.4 \pm 0.5$ MeV, $\Gamma_\rho = 146.5 \pm 0.8 \pm 1.5$ MeV and $\sigma(\rho \rightarrow \pi^+\pi^-) = 1220 \pm 7 \pm 16$ nb. The parameters of the G -parity suppressed process $e^+e^- \rightarrow \omega \rightarrow \pi^+\pi^-$ were measured with high precision. The measured value $\sigma(\omega \rightarrow \pi^+\pi^-) = 29.9 \pm 1.4 \pm 1.0$ nb corresponds to the relative probability $B(\omega \rightarrow \pi^+\pi^-) = 1.75 \pm 0.11\%$. The relative interference phase between the ρ and ω mesons was found to be $\phi_{\rho\omega} = 113.5 \pm 1.3 \pm 1.7$ degree. This result is in conflict with the naive expectation from the $\rho - \omega$ mixing $\phi_{\rho\omega} = 101^\circ$. The SND result agrees with the cross section calculated from the τ spectral function data within the accuracy of the measurements. Using measured cross section, the contribution to the anomalous magnetic moment of the muon due to the $\pi^+\pi^-(\gamma)$ intermediate state in the vacuum polarization was calculated: $a_\mu(\pi\pi, 390\text{MeV} \leq \sqrt{s} \leq 970\text{MeV}) = (488.7 \pm 2.6 \pm 6.6) \times 10^{-10}$.

Acknowledgments

The authors are grateful to N.N.Achasov for useful discussions. The work is supported in part by grants Sci.School-1335.2003.2, RFBR 04-02-16181-a, 04-02-16184-a, 05-02-16250-a.

-
- [1] H.N. Brown et al., Phys. Rev. Lett. **86**, 2227 (2001)
 - [2] G.W. Bennet et al., Phys. Rev. Lett. **92**, 161802 (2004)
 - [3] R. Barate et al., Z. Phys. C **76**, 15 (1997)
 - [4] K. Ackerstaff et al., Eur. Phys. J. C **7**, 571, (1999)
 - [5] S. Anderson et al., Phys. Rev. D **61**, 112002, (2000)
 - [6] J.E. Augustin et al., Phys. Rev. Lett. **20**, 126, (1968);
J.E. Augustin et al., Nuovo Cim. Lett. **2**, 214, (1969);
J.E. Augustin et al., Phys. Lett. **B28**, 508, (1969)
 - [7] V.L. Auslender et al., Phys. Lett. **B25**, 433, (1967);
V.L. Auslender et al., Yad. Fiz. **9**, 114, (1969) [Sov. J. Nucl. Phys. **9**, 69, 1969]
 - [8] D. Benaksas et al., Phys. Lett. **B39**, 289, (1972)
 - [9] A. Quenzer et al., Phys. Lett. **B76**, 512, (1978)
 - [10] I.B. Vasserman et al., Yad. Fiz. **28**, 968, (1978)
 - [11] A.D. Bukin et al., Phys. Lett. **B73**, 226, (1978)
 - [12] I.B. Vasserman et al., Yad. Fiz. **30**, 999, (1979)
 - [13] I.B. Vasserman et al., Yad. Fiz. **33**, 709, (1981) [Sov. J. Nucl. Phys. **33**, 368, 1981]
 - [14] L.M. Kurdadze et al., JETP Lett. **37**, 733, 1983 [Pisma Zh. Eksp. Teor. Fiz. **37**, 613, 1983]
 - [15] L.M. Kurdadze et al., Yad. Fiz. **40**, 451, (1984) [Sov. J. Nucl. Phys. **40**, 286, (1984)]
 - [16] S.R. Amendolia et al., Phys. Lett. **B138**, 454, (1984)
 - [17] L.M. Barkov, et al., Nucl. Phys. **B256**, 365, (1985)
 - [18] R.R. Akhmetshin et al, Phys. Lett. **B527**, 161, (2002);
R.R. Akhmetshin et al, Phys. Lett. **B578**, 285, (2004)
 - [19] A. Aloisio et al., Phys. Lett. **B606**, 12, (2005)
 - [20] M.N. Achasov et al., Nucl. Instr. and Meth. A **449**, 125 (2000)
 - [21] A.N. Skrinsky, in Proc. of Workshop on physics and detectors for DAΦNE, Frascati, Italy, April 4-7, 1995, p.3
 - [22] A.D. Bukin et al., in Proc. of Workshop on Detector and Event Simulation in High Energy Physics, p.79-85, 8-12 April 1991, NIKHEF, Amsterdam, Netherlands
 - [23] A.D. Bukin, N.A. Grozina, Comp. Phys. Comm. **78**, 287 (1994)
 - [24] K. Hanssger, S.Ritter, Comp. Phys. Comm. **31**, 411 (1984);
K. Hanssger, J.Ranft, Comp. Phys. Comm. **39**, 37 (1986);
K. Hanssger, J.Ranft, Comp. Phys. Comm. **39**, 53 (1986);
K. Hanssger, Nucl. Sc. and Eng. **95**, 137 (1987)
 - [25] A.D. Bukin, et al., Report No Budker INP 92-93, Novosibirsk, 1992
 - [26] F.A. Berends and R. Kleiss, Nucl. Phys. B **228**, 537 (1983)
 - [27] A.B. Arbuzov et al., JHEP 10, 001 (1997)
 - [28] A.B. Arbuzov et al., JHEP 10, 006 (1997)
 - [29] Bruce H. Denby, Comput.Phys.Comm. **49**, 429 (1988)
 - [30] M.N. Achasov et al., Phys. Rev. D **63**, 072002 (2001)
 - [31] M.N. Achasov et al., Phys. Rev. D **68**, 052006 (2003)
 - [32] M.N. Achasov et al., Phys. Rev. D **65**, 032002 (2002)
 - [33] S. Jadach, W. Placzek, B.F.L. Ward, Phys. Lett. B **390**, 298 (1997)
 - [34] A.V. Bogdan, et al., Report No Budker INP 2005-33, Novosibirsk, 2005
 - [35] J.Schwinger, Particles, Sources and Fields, vol.II, Addison-Wesley Publishing Company Advanced Book Program Reading, Massachusetts, 1973
M. Deers, K. Hikasa, Phys. Lett. B **252**, 127 (1990)
K. Melnikov, Int. J. Mod. Phys. A **16**, 4591 (2001)
A. Hoefler, J. Gluza, F. Jegerlehner, Eur. Phys. J. C **24**, 51 (2002)
 - [36] M.N. Achasov et al., Phys. Lett. B **559**, 171 (2003)
 - [37] N.N. Achasov, A.A. Kozhevnikov, and G.N. Shestakov, Phys. Lett. **50B**, 448 (1974) . N.N. Achasov, N.M. Budnev, A.A. Kozhevnikov, and G.N. Shestakov, Yad. Fiz. 23, 610 (1976) [Sov. J. Nucl. Phys. 23, 320 (1976)]; N.N. Achasov and G.N. Shestakov, Fiz. Elem. Chastits. At. Yadra 9, 48 (1978)
 - [38] N.N. Achasov and A.A. Kozhevnikov, Yad. Fiz. 55, 809 (1992) [Sov. J. Nucl. Phys. 55, 449 (1992)]; Int. J. Mod. Phys. A 7, 4825 (1992).
 - [39] D.Bisello et al., Phys. Lett. B **220**, 321 (1989)
 - [40] E. Braaten, S. Narison and A. Pich, Nucl. Phys. B **373**, 581 (1992)

- [41] A. Aloisio et al., Phys. Lett. **B561**, 55, (2003)
- [42] S. Eidelman et al., Phys. Lett. B **592**, 1 (2004)
- [43] P. Estabrooks and A.D. Martin, Nucl. Phys. B **79**, 301 (1974)
- [44] S.D. Protopopescu et al., Phys. Rev. D **7**, 1279 (1972)
- [45] M. Davier et al., Eur. Phys. J. C **27**, 497 (2003)
M. Davier et al., Eur. Phys. J. C **31**, 503 (2003)
- [46] N.N. Achasov, A.V.Kiselev, Pisma Zh. Eksp. Teor. Fiz. **75**, 643 (2002) [JETP Lett. **75**, 527 (2002)]